

Materials and Methods

Wounding experiments. All animal experiments were carried out in accordance with the guidelines of the IACUC of the University of Pennsylvania and the University of California, Irvine. Full thickness 1.5 x 1.5 cm (2.25cm²) excisional wounds were inflicted on the backs of three to eight week-old mice as previously described (2).

Phenotype quantification methodology. Whole mount wounds were stained for Oil Red O and the number of regenerated hair follicles was counted from the skin surface, where each new hair is clearly visible. The number of new adipocytes was counted from the underside, where each adipocyte is clearly visible due to their very large size and prominent marking by Oil Red O dye. For each experiment, adipose tissue regeneration was quantified as the ratio of all new adipocytes / all new hair follicles (*aka* adipocyte/hair follicle index). The index values for all experiments, statistical significance and number of biological replicates are summarized in the supplementary table S1. Some wound samples (Fig. 2B) were stained for lacZ and photographed, then additionally stained for Oil Red O and photographed again. Adipocytes were then micro-dissected and photographed under stereomicroscope.

Human scar cell isolation and culture. All human experiments were carried out in accordance with the guidelines of the IRB of the University of California, Irvine, Children's Hospital Los Angeles and Kyungpook National University. Keloid fibroblasts were isolated as previously described (23). Human hypertrophic scar myofibroblasts were derived from clinical specimen biopsies and expanded in vitro as previously described (24). All information pertinent to human scars is listed in supplementary table S2.

Primary mouse adipogenic cell culture. Primary scar cells were isolated from day 15 wound dermis as previously described (1) with minor modifications. Single cell fractions were created and cultured to confluence in high-glucose DMEM (Gibco) supplemented with 10% FBS (Atlanta Biologicals) and 10,000µl/ml Pen/Strep cocktail (Gibco). Upon confluency, cells were cultured in adipocyte differentiation media alone (Cell Solutions) or DMEM supplemented with 5µg/ml insulin (Sigma), and 1µM rosiglitazone (Sigma) with either 6ng/ml of recombinant hBMP4 (R&D Systems), or 25ng/ml of recombinant hBMP2 (R&D Systems). After three days

of induction, cells cultured in differentiation media were switched to adipocyte maintenance media (Cell Solutions). Cells were cultured in a water-jacketed incubator at 37°C with 5% CO₂ output.

Primary human adipogenic cell culture. Primary human scar cells were cultured in DMEM/F12 media (Gibco) supplemented with 10% FBS (Fisher Scientific). Upon confluency, cells were switched to serum free DMEM/F12 media and treated with 20ng/ml recombinant hBMP4 protein (R&D Systems) for 48 hours before differentiation. For the hair follicle coculture, cells were grown in 12-well trans-well plates. Once near confluency, medium was changed to William's E hair follicle organ culture medium (25), and 40 microdissected human scalp anagen hair follicles were cocultured on top of the membrane insert in each well for 5 days. Control cells were cultured in William's E medium without hair follicles. In all cases, adipogenic differentiation was induced by adding adipogenic cocktail: DMEM/F12 media supplemented with 1% ITS premix (insulin-transferrin-selenium; BD Biosciences), 0.5mM isobutylmethylxanthine (Sigma), 0.1mM cortisol (Sigma), 1mM dexamethasone (Sigma), 0.2nM triiodothyronine (Sigma), and 1mM rosiglitazone (Cayman Chemical). After 4 days of induction, cells were changed to maintenance media: DMEM/F12 media supplemented with 1% ITS premix (BD Biosciences), 0.1mM cortisol (Sigma), and 0.2nM triiodothyronine (Sigma). For the hair follicle coculture, cells were maintained in the induction media for 7 days. Lipid droplets were visualized after 7 days and cells were harvested for RNA isolation on day 10.

Murine stromo-vascular fraction (SVF) isolation. Visceral fat pads were dissected, minced and digested with 2.4U/ml collagenase and 1.5U/ml dispase mixture for 60 minutes at 37°C with constant agitation. Digestion was then stopped with MEM + 10% FBS. Cells were washed, filtered and centrifuged. Upon centrifugation, cells separate into two layers: fat-laden adipocytes at the top and SVF pellet at the bottom. The SVF pellet was collected and used in hair patch assays.

Hair patch assay. Epithelial and dermal cells were isolated from neonatal C57BL/6 mouse skin. 0.5×10^6 epithelial and 1×10^6 dermal cells were injected intradermally into *nu/nu* mice (Charles River). In some experiments, freshly isolated *Retn-lacZ* SVF cells were added. In other

experiments neonatal dermis was substituted by 1×10^6 of *Retn-lacZ* DP cells that were previously expanded for two weeks. The resulting patch assays were dissected and studied 14 days later.

Histology and immunohistochemistry. Immunostaining was performed on paraffin sections with heat-based antigen retrieval as required. The primary antibodies used were goat anti-ZFP423 (1:50; Abcam), rabbit anti-phospho-CEBP β ^{T188} (1:50; Cell Signaling), rabbit anti-PPAR γ (1:50; Cell Signaling), rabbit anti-Perilipin (1:750; Cell Signaling), rabbit anti-SMA (1:200; Abcam), mouse anti-PCNA (1:200; Abcam), rabbit anti-phospho-SMAD1/5/8 (1:50, Cell Signaling), rabbit anti-keratin K5 (1:250, Abcam), mouse anti- β -galactosidase (1:300; Developmental Studies Hybridoma Bank), mouse anti-Cre Recombinase (1:1000; Millipore), rabbit anti-tdTomato (1:1000; Rockland). Antibody masking was performed with donkey anti-rabbit whole IgG at 20ug/ml (Jackson ImmunoResearch) as required.

qRT-PCR. Total RNA was isolated using Trizol reagent (Thermo) or RNEasy Micro-Kit (Qiagen) as per manufacturer's protocol with minor modifications. Total RNA was reverse-transcribed and cDNA was amplified using PCR primers were previously described (8). See supplementary tables S3 and S4 for the sequence of primers used.

Fluorescence-activated cell sorting. Dorsal skin was collected from mice at different post-wounding time points. Scar tissue was micro-dissected, devoid of fascia and incubated in Dispase II solution (Sigma) to separate epidermis from dermis. Dermis was disaggregated into single cells with Collagenase IV (Sigma) at 37°C with constant rotation. Single cell fractions were stained with Zombie VioletTM (1:1000; BioLegend) and FACS-sorted as *Zombie^{neg};tdTomato^{hi}* with a BD FACSAria II flow cytometer (BD Biosciences) (fig. S12).

RNA isolation and SMART-seq2. Sorted, uncultured *Zombie^{neg};tdTomato^{hi}* myofibroblasts were re-suspended in RLT buffer supplemented with 1% beta-mercaptoethanol and homogenized with QIAshredder (Qiagen). Total RNA was isolated using the RNEasy Micro-Kit (Qiagen) as per manufacturer's protocol with minor modifications, including DNase I treatment (Qiagen). Optimal-quality RNAs were considered for cDNA library preparation (RIN>8.8). Full-length

cDNA library amplification was performed as previously described (26, 27). Briefly, 1ng total RNA was reversed-transcribed, and resulting cDNA was pre-amplified for 17 cycles. Tagmentation was carried out on 18ng cDNA using the Nextera DNA Sample Preparation Kit (Illumina). The Tn5 tagmentation reaction was carried out at 55°C for 5 minutes and purified using PCR Purification Kit (Qiagen). Adapter-ligated fragments were amplified using limited cycle enrichment PCR with Nextera barcodes for 7 continuous cycles, resulting libraries were purified with AMPure XP beads (Beckman Coulter). Library quantification was done using KAPA for Illumina sequencing platforms (Illumina). Libraries were multiplexed and sequenced as paired-end on a Next-Seq500 Illumina sequencing platform (Cluster density = 296K/mm², Clusters PF = 71.2%, Q30 = 87.6%).

SMART-seq2 analyses. Paired-end reads were aligned to the mouse reference genome (mm10/gencode.vM4) using bowtie (version 1.0.0) with default parameters. Transcripts were quantified using the RNA-seq by Expectation-Maximization algorithm (RSEM) (version 1.2.12) with the following default parameters: *rsem-calculate-expression -p \$SCORES --paired-end* (28). Samples displaying >20,000,000 mapped reads with >75% mapping efficiency were considered for downstream analyses. Differential expression dynamics across our single time experimental series was identified using the two-step regression model algorithm MaSigPro with a P-value cutoff of 0.05 for multiple hypothesis testing and a false discovery control rate of 0.01 (29, 30). Principle component analysis was performed using the R *ggbiplot* package. Data is available at GEO: GSE84256 (URL: <http://www.ncbi.nlm.nih.gov/geo/query/acc.cgi?acc=GSE84256>) and in data S1.

Meta-analyses. Transcriptome-wide meta-analyses was performed on microarray and RNA-seq datasets from skin-derived precursors (GEO: GSM464261) (31), *Nes-Cre*⁺ and *Nes-GFP*⁺ subcutaneous fat pericytes (GEO: GSM1573101) (32), E14.5 dermal fibroblasts (DFs) and dermal condensate cells (DCs) (GEO: GSE70288) (33), P5 dermal fibroblasts (DFs) and dermal papilla cells (DPs) (GEO: GSE77197) (34), P56 *Engr*⁺/*Engr*^{neg} fibroblasts (GEO: GSE65402) (18), P2 *Sca1*⁺/*Sca1*^{neg} fibroblasts (GEO: GSE76751) (35) and cutaneous myofibroblasts isolated from days 12, 15, 21 and 26 post-wounding (GEO: GSE84256). Processing of RNA-seq data sets: Reads from single-end data sets and single reads (read 1) from paired-end data sets were

trimmed to 43 bp. The trimmed reads were aligned to the mouse genome (mm10/gencode.vM9) using bowtie (version 1.0.0) with the following parameters: `--offrate 1 -a -m 200 --best -p 16 --seedlen 25 -n 2 -v 2`. Gene expression levels were obtained using RSEM (version 1.2.25) and used for the downstream analyses. Gene expression levels were transformed to *Z*-scores. Microarray data processing: All microarray data processing was performed in R (version 3.2.3) using corresponding Bioconductor packages. Raw microarray data were downloaded from GEO. Data normalization was done using the *rma* function of *affy* package. Median expression values were kept for genes that had multiple mapping probes. The gene expression levels from the microarray data sets were combined in a matrix and quantile-normalized using the *normalizeQuantiles* function of *limma* package. Gene expression levels were transformed to *Z*-scores. Combined RNA-seq and microarray data analyses: Gene expression *Z*-scores from RNA-seq and microarray data sets were combined into a matrix and batch-effect corrected using the *ComBat* function of *sva* package. Principle component analysis was performed using the *prcomp* function.

Supplementary Text

Supplementary Text S1: Additional lineage tracing results.

Several non-myofibroblast mesenchymal cell types display *SM22-Cre* and *SMA-CreER^{T2}* activity in and around the wound bed. These include vascular smooth muscle cells (VSMCs) of the wound and peri-wound blood vessels, subcutaneous skeletal muscle *panniculus carnosus* and dermal papilla cells of new hair follicles. To definitively establish that myofibroblasts are the key mesenchymal adipogenic progenitors in the wound we performed a series of additional lineage tracing experiments. First, we took advantage of the fact that not all smooth muscle contractile proteins are expressed in myofibroblasts. Smooth muscle myosin heavy chain (SMMHC *aka* MYH11) is expressed exclusively by true smooth muscle cells (36) and is distinctly absent from wound myofibroblasts (37). We performed lineage tracing in the wounds of *SMMHC-CreER^{T2};R26R* mice (38) using two induction protocols: 30 days before wounding to label pre-existing VSMCs of the cutaneous blood vessels and their progeny (n=4) (fig. S9A-B), and between days 11 and 17 after wounding to more specifically label VSMCs of the wound blood vessels (n=4) (fig. S9C-D). Upon analysis on day 28, lacZ activity remained restricted to wound and peri-wound blood vessels, and in all cases new adipocytes were not labeled.

Next, we traced the progeny of regenerating *panniculus carnosus* stem cells. Similar to other skeletal muscles, regeneration of *panniculus carnosus* is dependent on PAX7-expressing satellite stem cells. Intriguingly, a recent study that performed lineage tracing in *Pax7-Cre* mice concluded that upon wound healing *panniculus carnosus* satellite progenitors convert into dermal cells, and they constitute nearly a quarter of all cells in the newly formed scar tissue (39). However, more careful examination of *Pax7* promoter activity during development shows that it becomes exclusive to skeletal muscle lineage only after E12.5 and prior to that time point it is broadly active in dermomyotome precursors labeling dorsal dermis (40). Therefore, to achieve satellite stem cell specificity, we performed lineage tracing using an inducible *Pax7-CreER^{T2}* model (41). In *Pax7-CreER^{T2};R26R* mice that were induced one week prior to wounding we observed robust yet exclusive activation of lacZ expression in the regenerating muscle fibers of the *panniculus carnosus* at the wound edge with no contribution to the wound scar tissue (n=4) (fig. S9E).

Next, we tested adipogenic potential of dermal papilla cells from new hair follicles. During wound regeneration dermal papillae form before adipocytes and in *SM22-Cre* and *SMA-CreER^{T2}* mice they also activate reporter expression (fig. S7C, S8A', S11B). In normal hair follicles dermal papillae were reported to contain multipotent progenitors called skin-derived precursors (SKPs) that, among other lineages, can be induced to differentiate into adipocytes (31). A recent study showed that *CD133-CreER^{T2}* labeled dermal papilla cells of normal hair follicles do not contribute progeny toward wound scar tissue (42). To definitively address contribution of dermal papillae from new hair follicles toward new adipocytes, we performed wounding in *CD133-CreER^{T2};tdTomato* mice (43). Although normally *CD133-CreER^{T2}* is active in dermal papillae during hair follicle development and during first anagen phase of the hair cycle (42, 44), it becomes largely silenced during catagen and telogen phases. It also remains active in the endothelium of some blood vessels as judged by the expression of endogenous lacZ reporter contained within *CD133-CreER^{T2}* (fig. S10A). We show that *CD133-CreER^{T2}* becomes reactivated in the new hair follicles, providing a genetic tool for specific tracing of new dermal papilla cell progeny in the wound (fig. S10B). We now show that ten days after the induction of tdTomato expression in new dermal papillae of *CD133-CreER^{T2};tdTomato* mice, red fluorescent

cells continue to be restricted to new dermal papillae and no new adipocytes become labeled (n=7) (fig. S10C, S10D). Lastly, we tested the adipogenic potential of dermal papilla cells in the context of the so-called hair patch assay, which reproduces aspects of skin and hair follicle organogenesis from dissociated cells (45). Because neonatal skin contains many committed progenitors, including pre-adipocytes (46), patches generated with dissociated unsorted newborn mouse epidermis and dermis result in robust development of both hair follicles and fat (n=12) (fig. S10E). We then substituted newborn mouse dermis with vibrissa-derived dermal papilla cells from mice with lacZ knocked into the *Retn* locus. In these patches we observed formation of large vibrissa-like follicles and only occasional and always lacZ negative adipocytes (n=4) (fig. S10G). In contrast, the *Retn-lacZ* stromo-vascular fraction (SVF) cells were able to form lacZ positive adipocytes within patches (n=12) (fig. S10F), confirming the lack of adipogenic differentiation potential by dermal papillae cells in the context of hair follicle organogenesis. Taken together, the above lineage tracing studies help to define the in vivo adipogenic potential of various mesenchymal cells in the wound scar and also establish the role of myofibroblasts as the key adipogenic progenitors (fig. S9F).

Supplementary Text S2: Differential gene expression dynamics in cutaneous wound myofibroblasts.

Dermal fraction was isolated from dorsal cutaneous wounds of adult *SM22-Cre;tdTomato* mice and viable myofibroblasts were FACS-sorted as *Zombie^{neg};tdTomato^{hi}* from four post-wounding time points (fig. S12), including: (1) day 12 – initial wound closure and peak of myofibroblast presence, (2) day 15 – active formation of new hair follicles, (3) day 21 – appearance of ZFP423 expressing dermal progenitors juxtaposed to new hair follicles, and (4) day 26 – maturation of new adipocytes.

To resolve the transcriptome of cutaneous wound myofibroblasts we performed SMART-seq2 on RNAs isolated from viable, uncultured FACS-sorted *tdTomato^{hi}* myofibroblasts (26, 27). To identify unbiased gene expression profile changes in myofibroblasts across cutaneous regeneration, we conducted inferential statistical analyses using the two-step regression model algorithm maSigPro and identified 4,120 transcripts (approximately 10% of the vM4 gencode gene annotation list) that showed statistically significant differential expression across all four

time points analyzed ($P < 0.05$) (Fig. 3B; supplementary table S5) (29, 30). We analyzed the expression patterns of all differentially expressed genes using *K*-means clustering. These differentially expressed transcripts were grouped into five distinct clusters: (i) 1,412 transcripts in cluster C1 were high on days 12 and decreased by day 21, (ii) 1,244 transcripts in cluster C2 were high on days 12 and 15 and decreased significantly by day 26, (iii) 379 transcripts in cluster C3 transiently increased on days 15 and 21 relative to days 12 and 26, (iv) 688 transcripts in cluster C4 increased on days 21 and 26, and (v) 397 transcripts in cluster C5 increased on day 26 (Fig. 3B). Among the differentially expressed genes, the number of enriched cell cycle regulators significantly decreased during late post-wounding time points (compare small number of genes in clusters C3-C5 vs. these in C1 and C2; Fig. 3C). Similar temporal dynamics (i.e. decrease at late post-wounding time points) were observed for the enriched transcriptional regulators, epigenetic enzymes and inflammatory pathway genes. Contractile genes became downregulated after day 15, consistent with the shutdown of the active contractile state by myofibroblasts during late wound healing stages. The number of enriched extracellular matrix and secreted/signaling pathway genes showed a prominent increase at times coinciding with wound adipogenesis, days 21 and 26 (in cluster C4; Fig. 3C). Principal component analysis (PCA) of differentially expressed genes showed myofibroblasts from individual stages clustering closely together (Fig. 3A; fig. S13), corroborating that pooled populations of myofibroblasts isolated across wound regeneration display unique and dynamic transcriptomic profiles.

Supplementary Text S3: Changes in transcriptional regulators.

A number of transcriptional regulators previously implicated in adipogenesis show expression changes consistent with the activation of adipogenic lineage commitment at late post-wounding time points (fig. S14). Known modulators of adipogenesis, including negative regulators *Nr2f6* (-1.4x) (47) and *E2f4* (-2.1x) (48) were downregulated (clusters C1 and C2 accordingly), while *Zfp423* (+2.6x) (9, 10, 49-52), *Crebl2* (+1.9x) (53), *Stat5b* (+1.7x) (54-56), and *Klf15* (+2.6x) (57, 58) were upregulated (clusters C4 and C5). Here and below, the day 26 vs. day 12 fold ratio is shown. Concomitant with the above changes in adipose lineage regulators, expression changes were observed for several key transcriptional regulators of alternative mesenchymal lineages, including chondrogenic and osteogenic (fig. S14). Prominently downregulated were *Sox9* (-2.7x) (59-62), *Sox11* (-2.4x) (63), *Fhl2* (-2.4x) (64-66), *Runx1* (-2.9x) (67, 68), *Runx2* (-3.2x) (69-71),

Glis3 (-3.3x) (72), and *Pitx1* (-2.1x) (73). Of note, key transcriptional regulators of the myogenic lineage, *Pax3*, *Pax7*, *Myf5*, *Myf6*, and *Myod* were not differentially expressed in our time course analyses ($P > 0.05$).

Supplementary Text S4: Changes in major signaling pathways.

The above-described changes in transcriptional regulators were accompanied by substantial changes in several major signaling pathways associated with adipose lineage regulation (fig. S14). Signaling members of the pro-adipogenic bone morphogenetic protein (BMP) pathway (74-76) showed changes consistent with BMP activation at late post-wounding stages, on days 21-26. Prominently, BMP antagonists *Bambi* (-1.6x) and *Grem1* (-3.5x) were downregulated (cluster C1), while BMP ligands *Bmp4* (+5.0x) and *Bmp7* (+7.4x) became upregulated (cluster C4). *Id1* (+2.0x) and *Id2* (+1.7x), known direct BMP targets, also were upregulated on day 26 (cluster C5). Also, BMP receptor *Bmpr1a* was transiently upregulated on days 15 and 21 (cluster C3).

Opposite dynamics were observed for the members of the canonical Wnt signaling pathway, which is largely associated with the inhibition of adipogenesis (77-79) (fig. S14). Wnt ligands, *Wnt2b* (-3.8x) and *Wnt7b* (-1.2x) became downregulated (cluster C1), while soluble Wnt antagonists *Dkk2* (+14.3x), *Wif1* (+32.5x) and *Sfrp4* (+2.3x) became upregulated during late post-wounding stages (cluster C4). Inhibitory effect of SFRP4 on adipogenesis has been previously demonstrated in vitro (80). Furthermore, downregulated during late stages were the intracellular signaling mediators of Wnt, including *Foxk1* (-1.5x) (81), *Ctnnb1* (-1.3x), *Tcf19* (-2.1x) and *Lypd6* (-1.9x) (82). Importantly, higher levels of canonical Wnt signaling on days 12-15 are consistent with our earlier report on the activation of canonical Wnt signaling in wound myofibroblasts at the onset of new hair follicle regeneration (1). At late stages (cluster C4), we also observe an upregulation of *Wnt5b* (+2.7x) and *Wnt16* (+3.4x), both of which have been shown to act as non-canonical Wnt ligands. Promoting effect of non-canonical Wnt signaling on adipogenesis, in particular WNT5b, has been documented in vitro (83-85).

Among other pathways (fig. S14), fibroblast growth factor (FGF) pathways show distinct gene expression patterns during late stages. Several FGF ligands were upregulated, including *Fgf9*

(+3.6x), *Fgf11* (+1.7x), *Fgf14* (+1.9x) in cluster C4 and *Fgf10* (+3.1x) in cluster C5. Also upregulated were FGF receptors *Fgfr2* (+3.0x) and *Fgfr4* (+5.7x) in cluster C4 and FGF binding protein *Fgfbp1* (+11.3x) in cluster C5. Previously, FGF10 has been shown to stimulate proliferative expansion of adipose progenitors (86-88). Dynamic changes are also observed for the insulin/insulin growth factor (IGF) signaling pathway. Prominently, ligand *Igf2* (-19.8x), its receptor *Igf2r* (-2.1x) and modulator of translation *Igf2bp2* (-4.1x) became downregulated in late stages (cluster C2). In line with our observations, previous reports suggest that a decrease in IGF2 levels is associated with increased fat deposition and occasional obesity (89, 90). Moreover, IGF2 inactivation, along with MYOD (not differentially expressed), was shown to be essential for brown fat vs. skeletal muscle cell fate selection (91).

Among other established and differentially expressed regulators of adipogenesis (fig. S14), *Dkl1* (-10.5x) (92-98) and *Mest* (-23.9x) (99), known negative regulators, were downregulated (cluster C2), while *Agouti* (+2.2x) (100, 101), known positive regulator, was upregulated (cluster C5). Also prominently upregulated in clusters C4 was adipokine *Wisp2* (+21.3x) (13, 102, 103), known to be highly expressed by adipose precursor cells (13).

Supplementary Text S5: Changes in the epigenetic regulators.

A number of changes are also observed in the expression of known epigenetic enzymes (fig. S14). Numerous epigenetic enzymes broadly associated with global transcriptional repression were downregulated during late time points. These include histone deacetylase *Hdac9* (-2.1x) and histone deacetylase complex subunit *Sap30* (-4.5x). Also downregulated were several histone methyltransferases, including *Ezh2* (-2.4x), the key catalytic subunit of the Polycomb repressive complex 2, and *Whsc1* (-3.4x), both of which catalyze deposition of the repressive H3K27me marks (mono-, di- and tri-), and *Suv39h1* (-2.9x), which catalyzes deposition of the repressive H3K9me3 marks. Other downregulated transcriptional repressors were polycomb group ring finger protein *Pcgf2* (-2.1x), chromobox protein homolog *Cbx5* (-2.2x), and prominently, DNA methyltransferase *Dnmt1* (-2.3x). Among these factors, inhibitory effects during adipogenesis were shown for HDAC9 (104-107) and SUV39H1 (108). DNMT1 was shown to become downregulated during adipocyte differentiation in vitro, and its siRNA-mediated knockdown in pre-adipocytes induces premature differentiation (109). Among other

epigenetic modifiers with at least two-fold change in expression were putative histone methyltransferase *Prdm6* (+2.5x) in cluster C4 and chromatin remodeling protein *Chd5* (+2.6x) in cluster C5.

Supplementary Text S6: Meta-analysis of myofibroblasts' transcriptome profile.

To gain further insight into the possible relation between wound myofibroblasts and dermal cells from unwounded skin, we compared the RNA-seq profiles of myofibroblasts with previously reported RNA-seq and microarray data sets from various dermal cell populations using principal component analyses (PCA) (see “Meta-analyses” section of the Materials and Methods for details) (fig. S15). We observe close association between *Nes-Cre⁺/Nes-GFP⁺* subcutaneous fat pericytes, P56 *Engr⁺/Engr^{neg}* dermal fibroblasts, and P2 *Sca1⁺/Sca1^{neg}* reticular and papillary dermal fibroblasts, suggesting negligible variance between their transcriptomes, but otherwise significant transcriptome variance relative to other dermal cells, including wound myofibroblasts from all time points. Recently, *Engr⁺* fibroblasts (EPFs), but not *Engr^{neg}* fibroblasts (ENFs) were shown to be the predominant type of scar-forming fibroblasts in small excisional skin wounds in adult mice (18). Our PCA suggests significant transcriptome variance between myofibroblasts in large wounds and *Engr⁺/Engr^{neg}* dermal fibroblasts, suggesting that myofibroblasts undergo significant transcriptome changes following wounding. *Sca1⁺* reticular dermal fibroblasts were recently described as having a pre-adipocyte gene signature, validated in vitro by their ability to undergo adipocyte differentiation (35). Significant transcriptome variance between myofibroblasts and *Sca1⁺* dermal cells does not support a close relationship. We also compared myofibroblasts to skin-derived precursors (SKPs) and *Sox2⁺* dermal papilla cells (the primary source of SKPs in adult mouse skin). Both SKPs and *Sox2⁺* dermal papilla cells were reported to be multipotent based on their ability to differentiate in vitro and in cell transplantation assays into several mesenchymal cell types, including adipocytes, as well as several types of neuronal cells, peripheral neurons and Schwann cells (31). However, a recent study (42) and our lineage studies (see supplementary text S1) show no contribution from pre-existing and new dermal papilla cells toward wound scar tissue and new adipocytes. In parallel, we also see high transcriptome variance between SKPs, *Sox2⁺* dermal papilla cells and myofibroblasts from all time points. Together, our lineage tracing and reconstitution patch assays (fig. S10) coupled with transcriptome-wide meta-analyses (fig. S15) suggest that multipotent precursors of the dermal

papilla are the unlikely source of new adipocytes. Importantly, on PCA analysis, E14.5 dermal fibroblasts (DFs) and dermal condensate cells (DCs) (33) cluster in close proximity to day 12 and 15 myofibroblasts, while P5 dermal fibroblasts (34) cluster close to day 21 and 26 myofibroblasts. These results are in line with the notion that: (i) the transcriptomes of myofibroblasts in adult regenerating wounds undergo changes similar to these in dermal fibroblasts during skin morphogenesis, and (ii) that wound myofibroblasts reprogram toward a distinct regeneration-competent state.

Supplementary Text S7: Adipogenic conversion of human scar fibroblasts in vitro.

Human cells derived from keloid (n=3) and hypertrophic scars (n=3; supplementary table S2) were subjected to adipogenic culture (see Materials and Methods). Cells were pre-treated with hBMP4 for 48 hours in an attempt to induce BMP-mediated adipogenic commitment, and then differentiated using standard adipogenic cocktail. As judged by the appearance of Oil Red O positive cells with typical adipocyte morphology, these culture conditions consistently induced adipogenic conversion of keloid (Fig. 4C), but not hypertrophic scar cells (fig. S22). Adipogenic conversion of keloid scar fibroblasts was accompanied by the upregulation of adipogenic genes, *ZNF423* (human *Zfp423* homolog), *ADIPOQ*, *ADIPOSIN*, *PPARG2*, *FABP4* (Fig. 4D). Importantly, adipogenic potential of both hypertrophic and keloid scar cells without hBMP4 treatment was low. Next, to test if anagen hair follicles are sufficient to induce adipogenic conversion of human keloid cells, we cocultured them with freshly microdissected human scalp anagen hair follicles for five days prior to inducing adipogenic differentiation. To prevent possible contamination of keloid cell culture with hair follicle-derived cells, the latter were cultured on top of an insert that prevents cell migration (see Materials and Methods; fig. S22E). We show that hair follicle coculture is sufficient to substitute for hBMP4 and it induces adipogenic conversion of keloid cells, as judged by the formation of BODIPY-positive lipid-containing adipocytes (Fig. 4E) and activation of adipogenic gene expression (Fig. 4F). Together, these results indicate partial conservation of the BMP-ZFP423 adipogenic reprogramming pathway in human keloid scar cells and also show that hair follicles are sufficient to induce adipogenic reprogramming.

Supplementary Figures

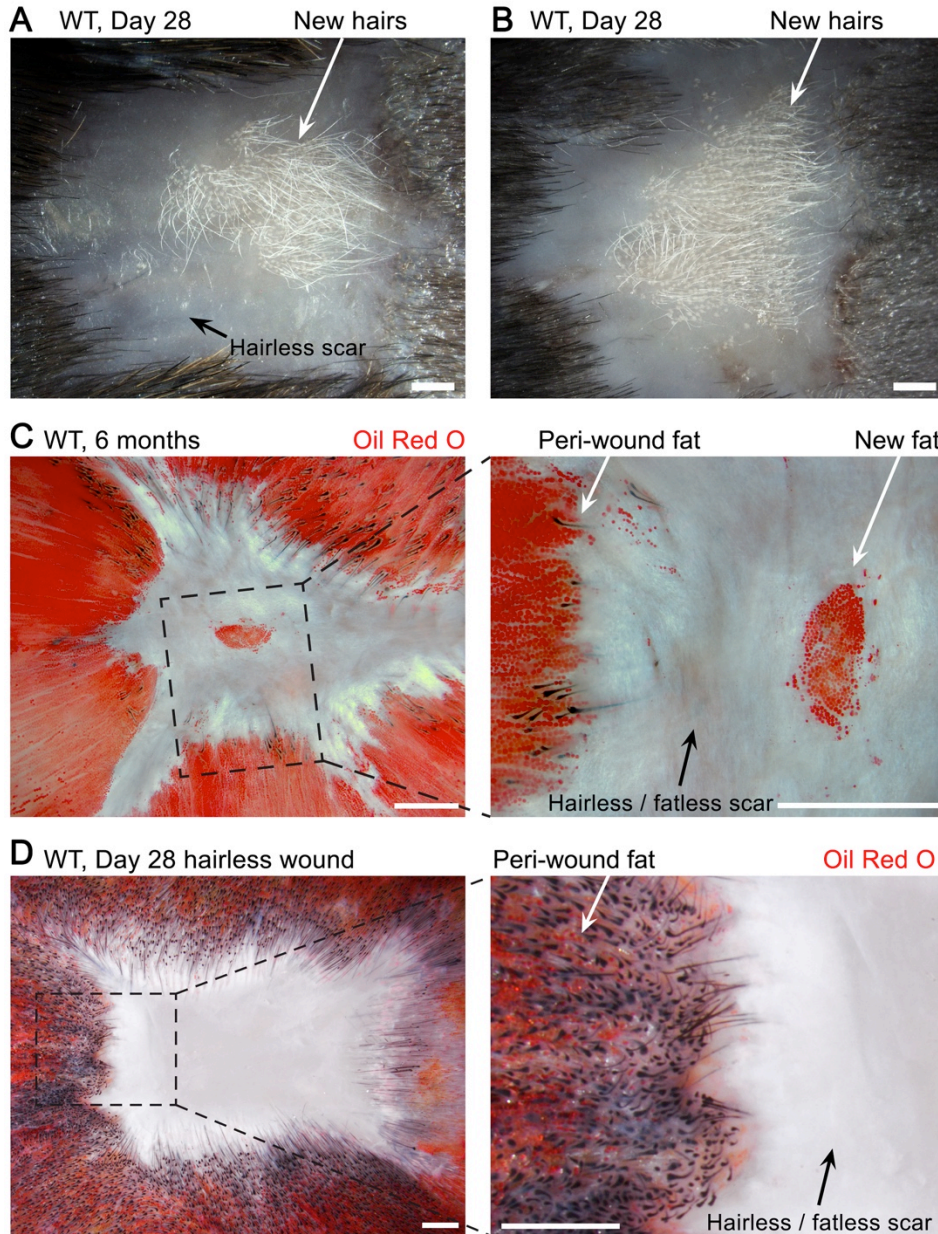


Fig. S1: Wound induced new hair follicles and new fat. (A-B) View from skin surface. In large wounds, many new hair follicles regenerate in the center and commonly lack pigmentation. **(C) View of underside of skin.** New adipocytes are maintained 6 months post-wounding in close physical proximity to new hair follicles and not in the hairless portions of the scar (enlargement is rotated). **(D)** New adipocytes do not regenerate in hairless wounds. Wound samples were stained for Oil Red O to detect adipocytes. Scale bars in (A) to (D), 1 mm.

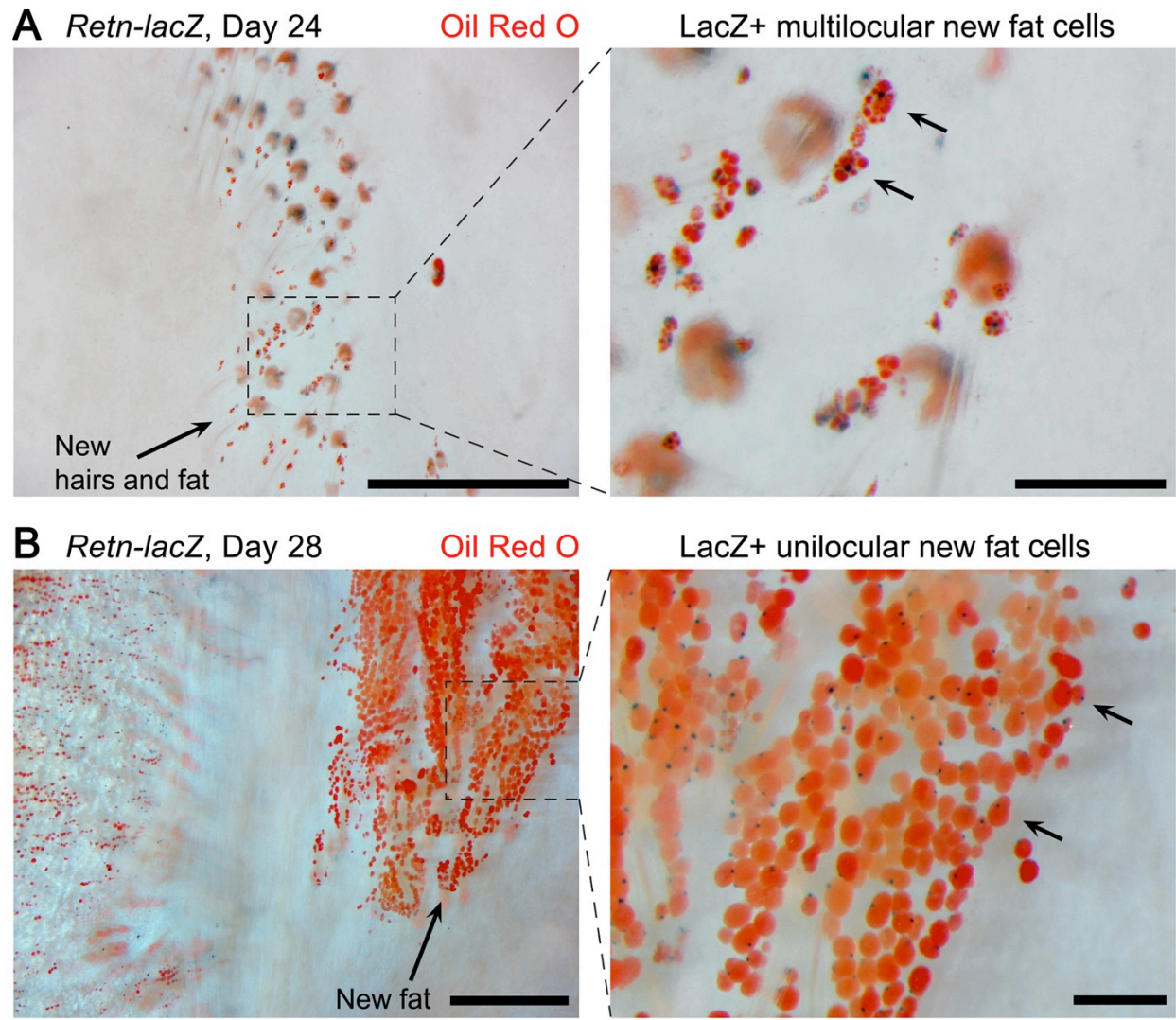


Fig. S2: Maturation of new adipocytes. On day 24 new adipocytes have a multilocular morphology (**A**), but acquire a unilocular morphology by day 28 (**B**). *Retn-lacZ* wound samples were stained for lacZ (nuclear localization, arrows) and counterstained for Oil Red O. **Views of underside of skin.** Scale bars in left panels, 1 mm; in right panels, 200 μ m.

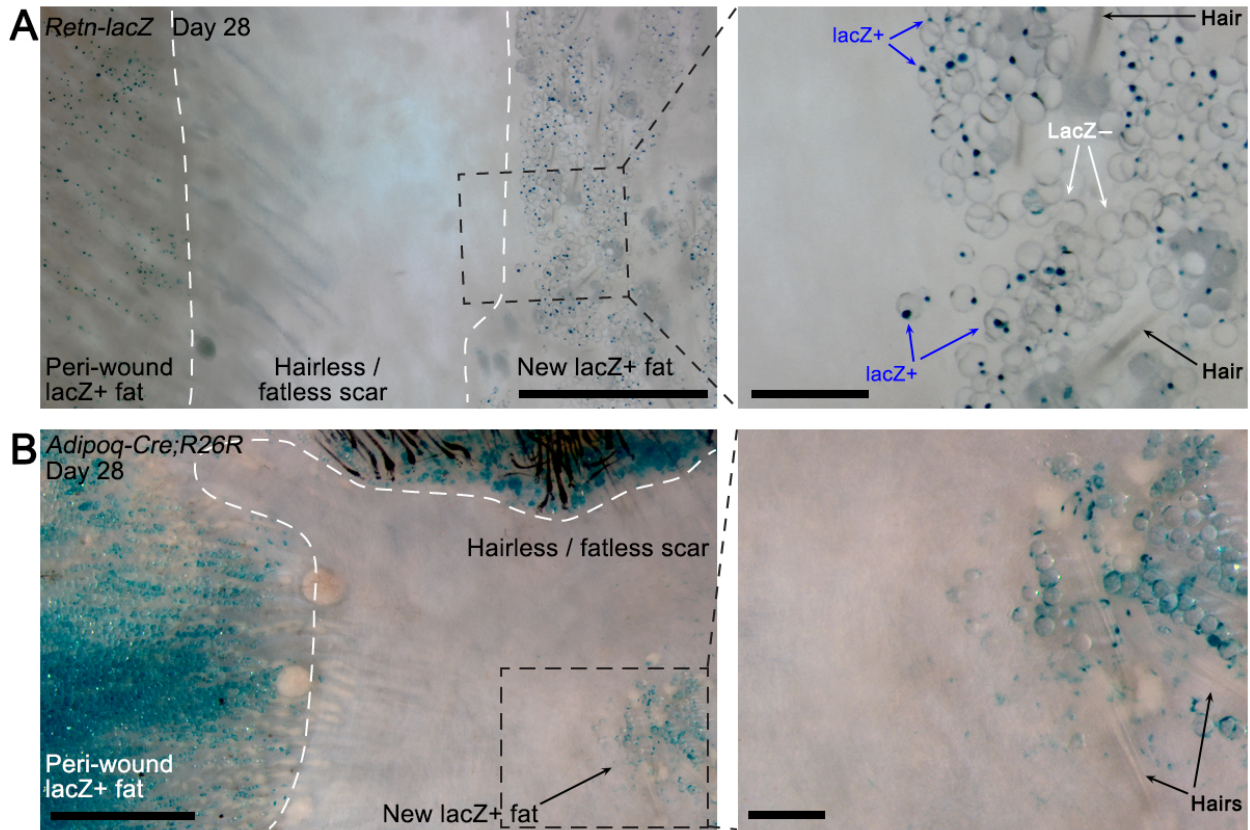


Fig. S3: New adipocytes express the fat-specific hormones resistin and adiponectin. (A) Similar to normal skin adipocytes, new adipocytes in the wound express the fat-specific hormone resistin as seen in *Retn-lacZ* mice expressing nuclear lacZ. **(B)** In the skin of *Adipoq-Cre;R26R* mice, both normal adipocytes at the wound edge and new adipocytes in the wound center express lacZ. Note lack of lacZ positive cells in hairless portion of the scar. **Views of underside of skin.** Scale bars in left panels, 1 mm; in right panels, 200 μ m.

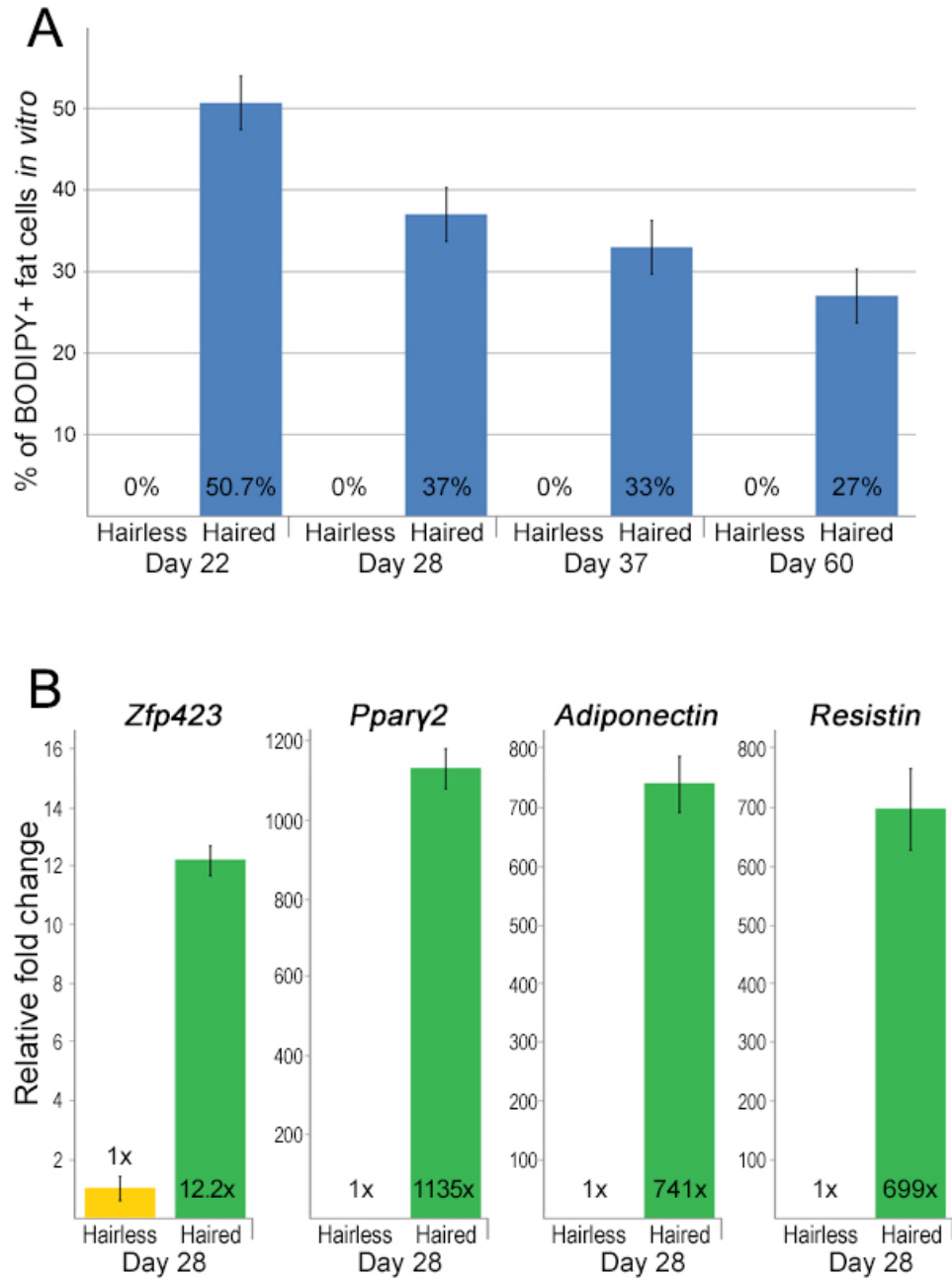


Fig. S4: New adipocytes only regenerate around new hair follicles. (A) Quantitation of adipocytes as percentage of total cultured dermal cells from haired and hairless wounds at different times. **(B)** In vitro adipogenesis confirmed by differential expression of white adipose-specific genes, *Zfp423*, *Pparg2*, *Adiponectin*, *Resistin*.

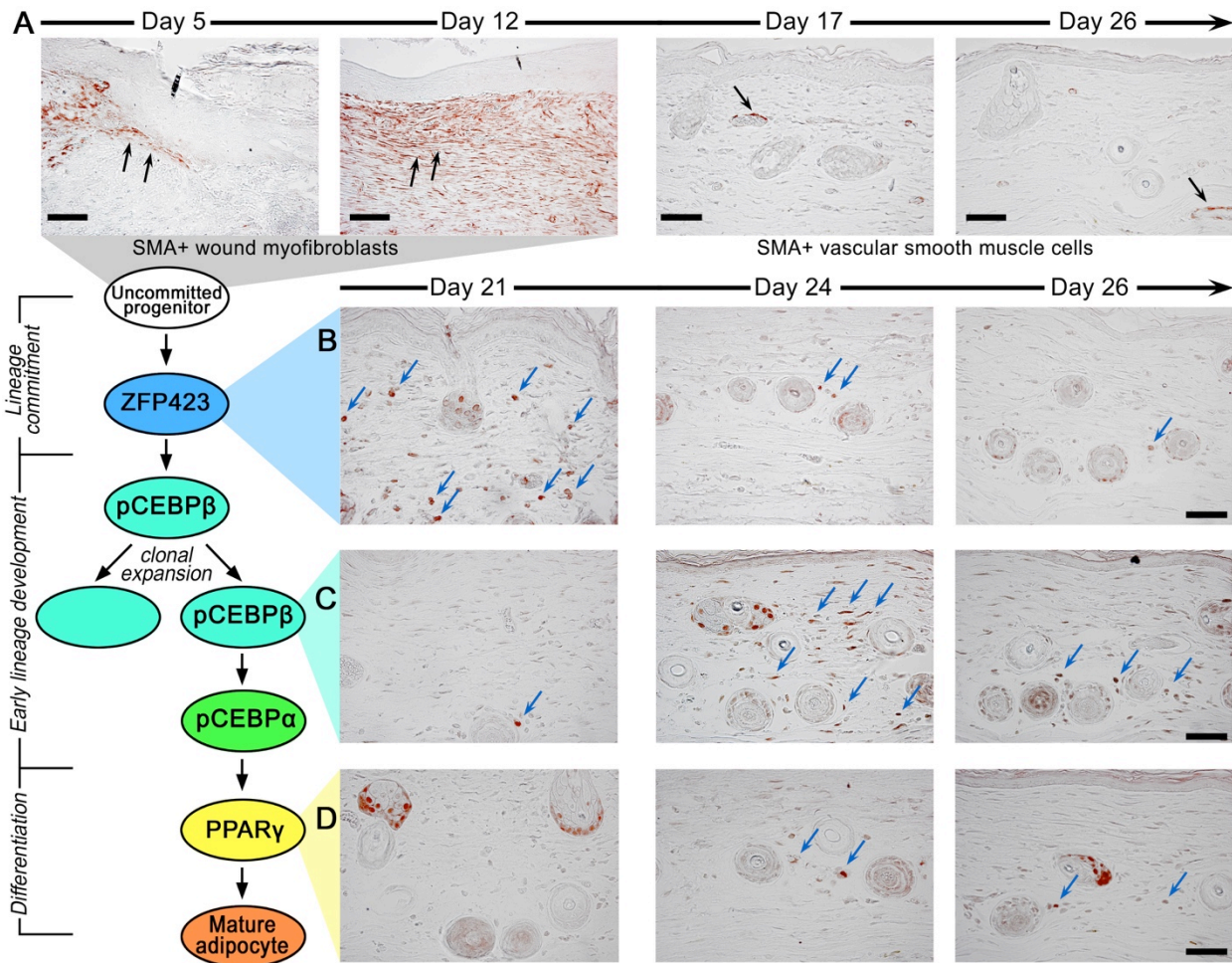


Fig. S5: New adipocytes temporally express characteristic developmental markers for adipocytes. (A) SMA positive myofibroblasts are present at the wound edge at day 5 and then in the wound center at day 12. By day 17, dermal cells express very little SMA. On days 21 and 24, dermal cells expressing adipocyte precursor markers, ZFP423 and pCEBP β , (B, C), and then the adipocyte differentiation marker, PPAR γ , appear sequentially (D). Note that panel A is identical to the panel A on main Fig. 2 (same data). Scale bars in (A) to (D), 100 μ m.

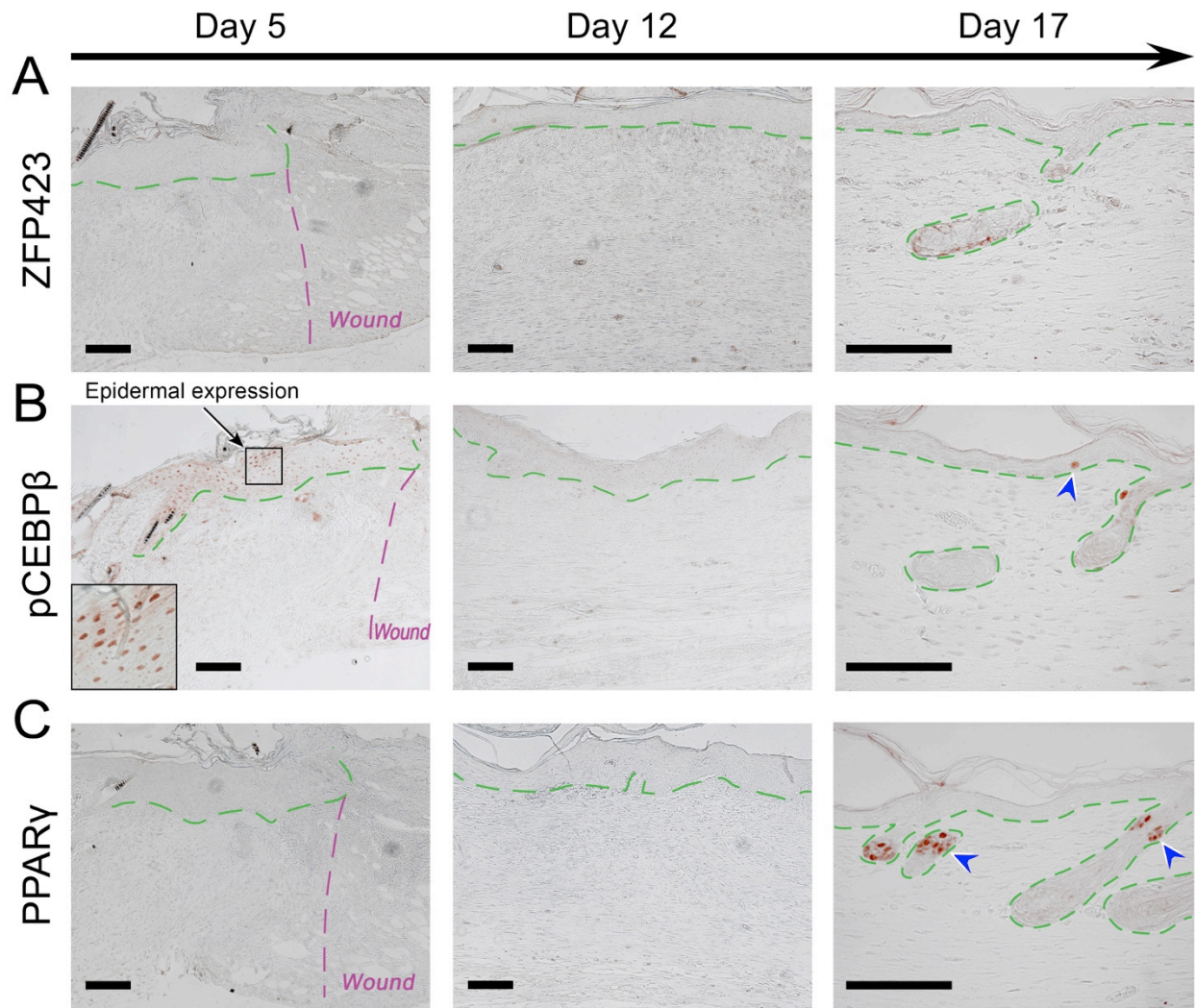


Fig. S6: Expression of adipogenic markers in early stage wounds. ZFP423 (A), pCEBP β (B) and PPAR γ (C) are not expressed in large skin wounds on days 5, 12 and 17. Blue arrowheads mark expression in epithelial compartments, including epidermis and sebaceous glands. Scale bars in (A) to (C), 100 μ m.

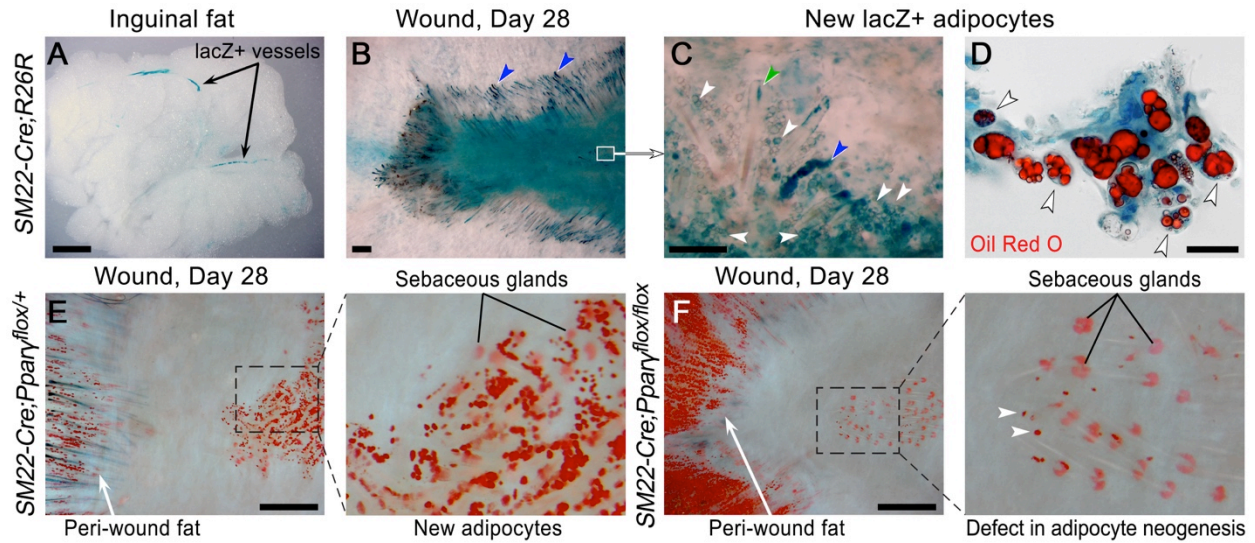


Fig. S7: New adipocytes in the wound arise from *SM22-Cre* positive cells. (A-D) New adipocytes (white arrowheads in C and D) express lacZ in *SM22-Cre;R26R* mice. This contrasts with the lack of expression in normal cutaneous (B) and visceral fat cells (A). Other expression sites of *SM22-Cre* in the wound include blood vessels, dermal papillae (green arrowhead in C) and epithelial outer root sheath of some wound and peri-wound hair follicles (blue arrowheads on B and C). LacZ positive new adipocytes in D were counterstained for Oil Red O. (E, F) *SM22-Cre* driven deletion of *Pparγ* results in the near complete loss of new adipocytes, while normal skin adipocytes at the wound edge develop properly. Formation and growth of new hair follicles in *SM22-Cre;Pparγ^{flox/flox}* mice is largely unaffected. Wound samples were stained for Oil Red O. **Views of underside of skin.** Scale bars in (A), (B), (E) and (F), 1 mm; in (C), 200 μ m; in (D), 50 μ m.

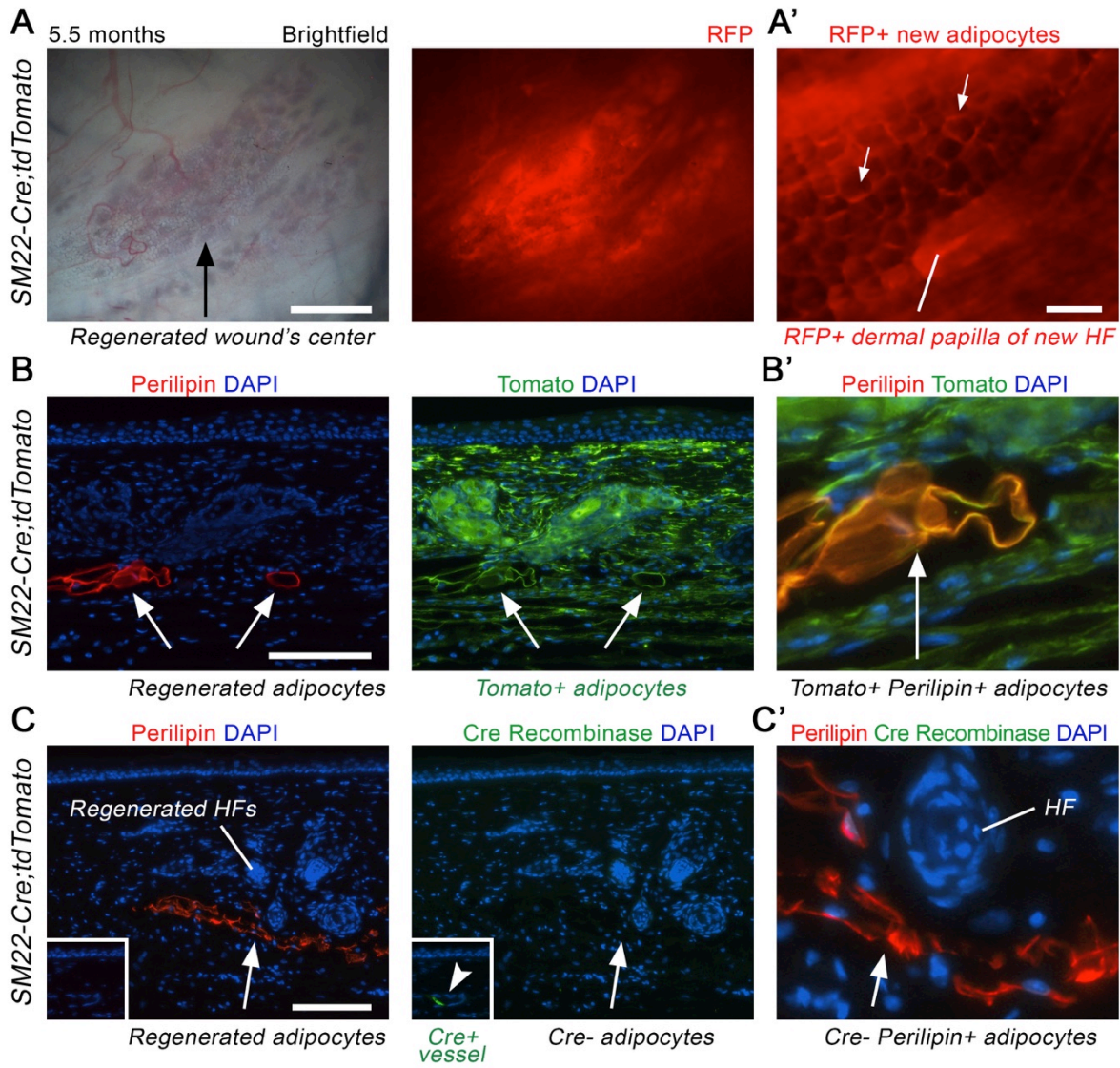


Fig. S8: *SM22-Cre* expressing cells give rise to new adipocytes in the wound. (A, A') New adipocytes (white arrows in A') express red-fluorescent reporter in *SM22-Cre;tdTomato* mice indicating that they originate from myofibroblasts. **Views of underside of skin.**

(B, B') New adipocytes in *SM22-Cre;tdTomato* wounds (white arrows) co-express adipocyte marker Perilipin (red) and tdTomato (green) confirming that they originate from myofibroblasts.

(C, C') New Perilipin-positive adipocytes (red) in *SM22-Cre;tdTomato* wounds do not co-express Cre Recombinase (green) confirming that cells no longer activate *Sm22-Cre*. Insert shows positive Cre Recombinase expression (green) on the blood vessel in the wound. Scale bars in (A), 1 mm; in (A'), 200 μ m; in (B) and (C), 100 μ m.

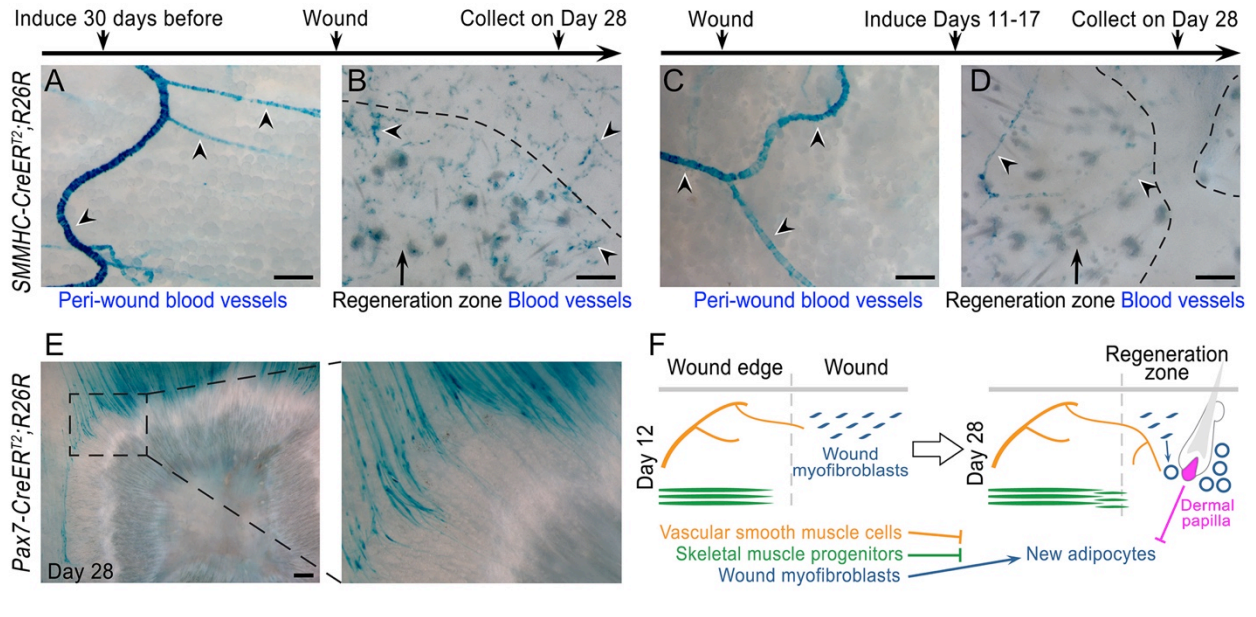


Fig. S9: Among wound myofibroblasts, vascular, and muscle cells adjacent to the wound, only wound myofibroblasts give rise to new adipocytes. (A-D) SMMHC expressing vascular smooth muscle cells do not contribute to new adipocytes as confirmed by lineage tracing in the wounds of *SMMHC-CreER^{T2};R26R* mice induced either 30 days prior to wounding (**A, B**) or between days 11-17 after wounding (**C, D**). With both induction protocols, lacZ positive cells remain restricted to wound and peri-wound blood vessels (arrowheads). **(E)** PAX7 expressing satellite stem cells of the *panniculus carnosus* muscle do not contribute to new adipocytes as confirmed by lineage tracing in the wounds of *Pax7-CreER^{T2};R26R* mice induced one week prior to wounding. LacZ labeled cells remain restricted to regenerating skeletal muscle fibers. **(F)** Schematic representation of contractile cell types in and around regenerating wounds. Among heterogeneous contractile cell types, only wound myofibroblasts contribute progenitors toward new fat tissue. **Views of underside of skin.** Scale bars in (A) to (D), 200 μ m; in (E), 1 mm.

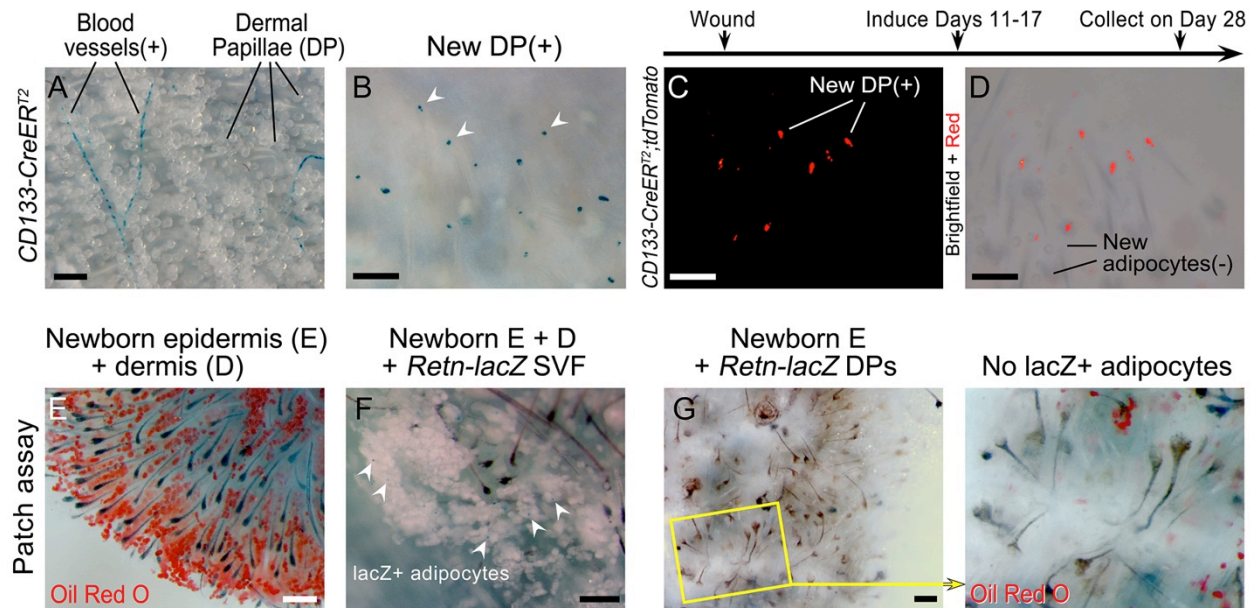


Fig. S10: Dermal papillae of new hair follicles do not possess adipogenic progenitor potential. (A, B) Activity of endogenous lacZ reporter in adult *CD133-CreER^{T2}* mice is restricted to isolated cutaneous blood vessels and to dermal papillae of new (white arrowheads), but not normal peri-wound hair follicles. (C, D) CD133 expressing new dermal papilla cells do not contribute to new adipocytes as confirmed by lineage tracing in the wounds of *CD133-CreER^{T2};tdTomato* mice induced between days 11-17 after wounding. On day 28, tdTomato labeled cells remain restricted to dermal papillae of new follicles and do not convert into new adipocytes.

(E-G) In a hair follicle reconstitution assay, *Retn-lacZ* vibrissa-derived dermal papilla cells induce formation of new follicles, but do not give rise to lacZ positive adipocytes (G). In contrast, *Retn-lacZ* WAT stromo-vascular fraction cells contribute lacZ positive adipocytes into reconstituted skin generated with newborn dermis and epidermis (F, arrowheads). Samples on E and G (right panel only) were counterstained for Oil Red O. **Views of underside of skin.** Scale bars in (A) to (G), 200 μ m.

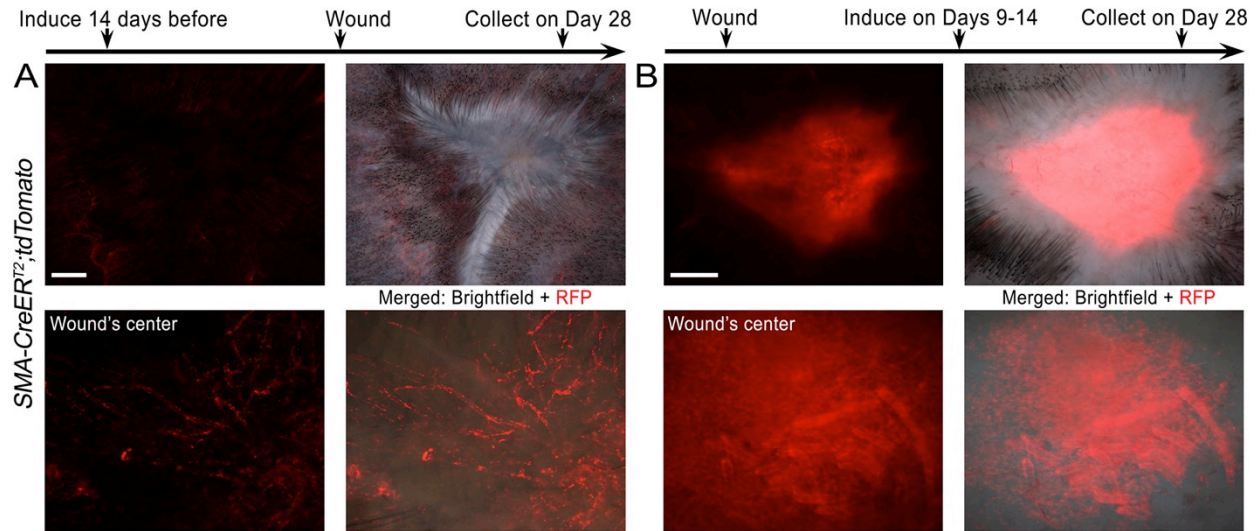


Fig. S11: *SMA-CreER^{T2}* can be used to lineage trace wound myofibroblasts. (A) Cre induction in *SMA-CreER^{T2};tdTomato* mice 14 days before wounding results in preferential labeling of vascular smooth muscle cells. **(B)** Induction during days 9-14 after wounding results in labeling of myofibroblasts in the wound center. **Views of underside of skin.** Scale bars in (A) and (B), 2 mm.

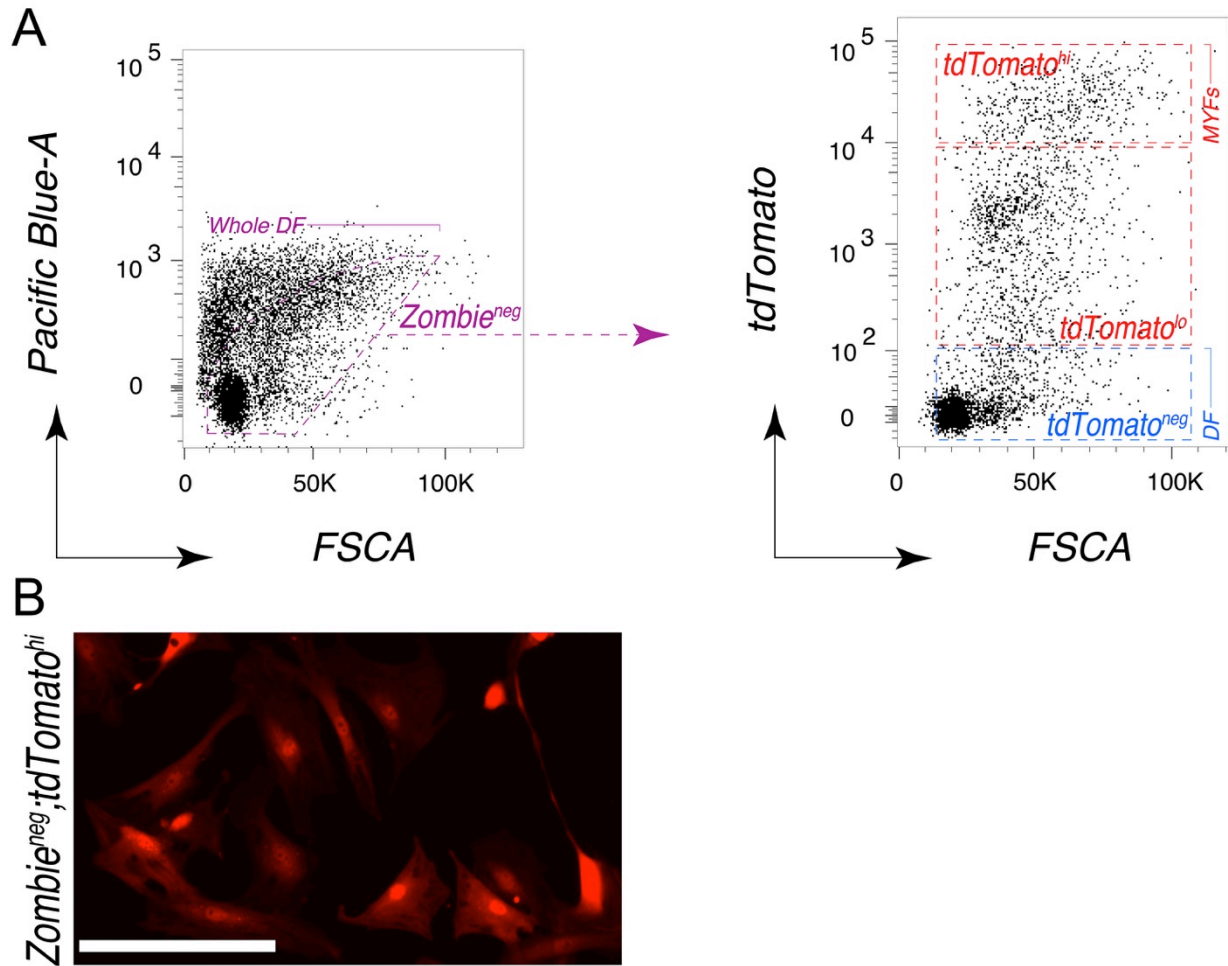


Fig. S12: Sorting strategy for wound myofibroblasts. (A) Schematic representation of sequential FACS gating of wound myofibroblasts. Single dermal fractions (DF) from *SM22-Cre;tdTomato* mouse wounds were gated on viable cells (*Zombie^{neg}*). *tdTomato⁺* populations were classified as *tdTomato^{lo}* and *tdTomato^{hi}*. (B) *tdTomato^{hi}* cells displayed large size, prominent spindle-shaped morphology and high *tdTomato* expression. Scale bars in (B), 200 μ m.

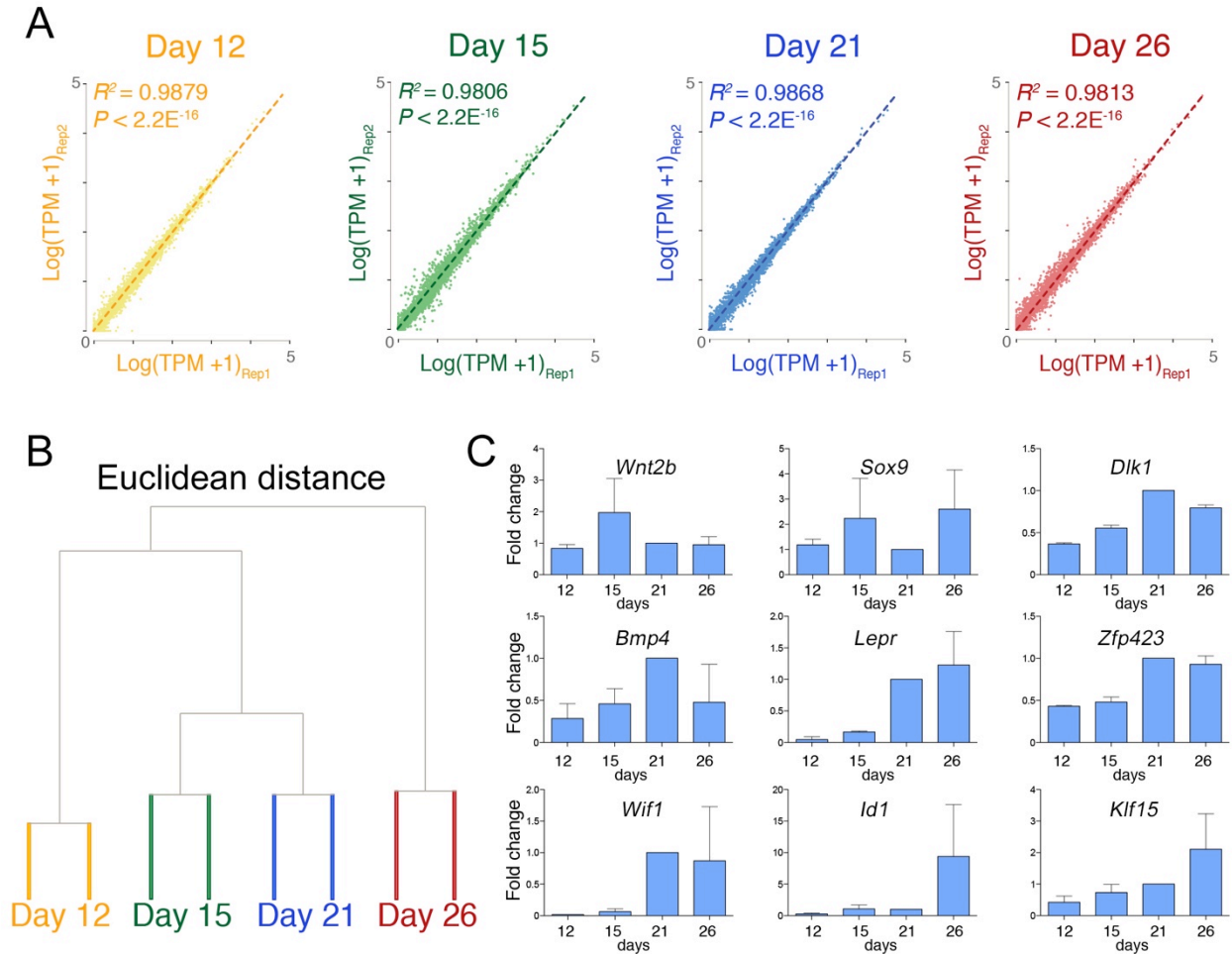


Fig. S13: Analyses of myofibroblast RNA-sequencing data during wound healing. (A) Spearman correlation coefficients for gene expression profiles of biological replicates. **(B)** Hierarchical clustering of myofibroblasts based on Euclidean distance. **(C)** qRT-PCR against select genes in sorted cutaneous myofibroblasts at different time points post-wounding (n=2 for each time point). Values in the graphs are means \pm SEM normalized to post-wounding day 21.

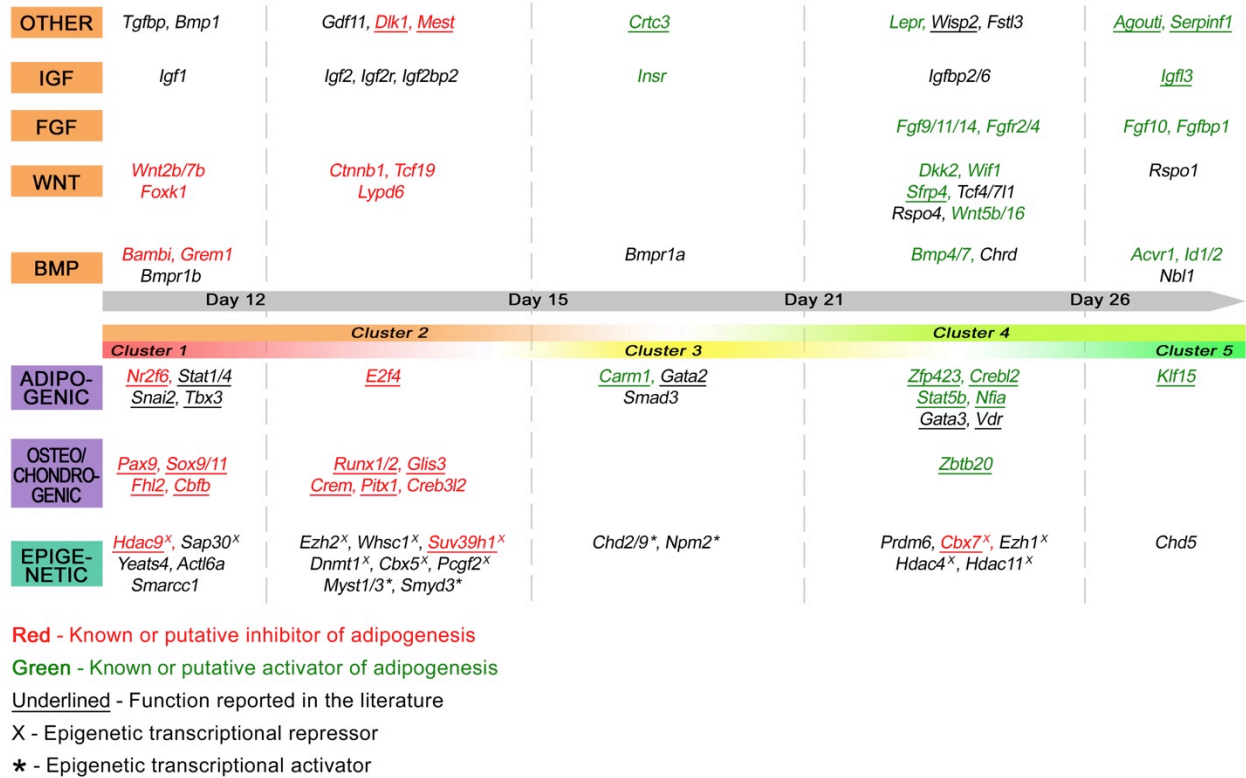


Fig. S14: Gene expression changes in myofibroblasts during wound healing reflect their conversion to adipocytes. Adipogenic inhibitors are highly expressed at early time points whereas, in later time points, activators of adipogenesis are highly expressed.

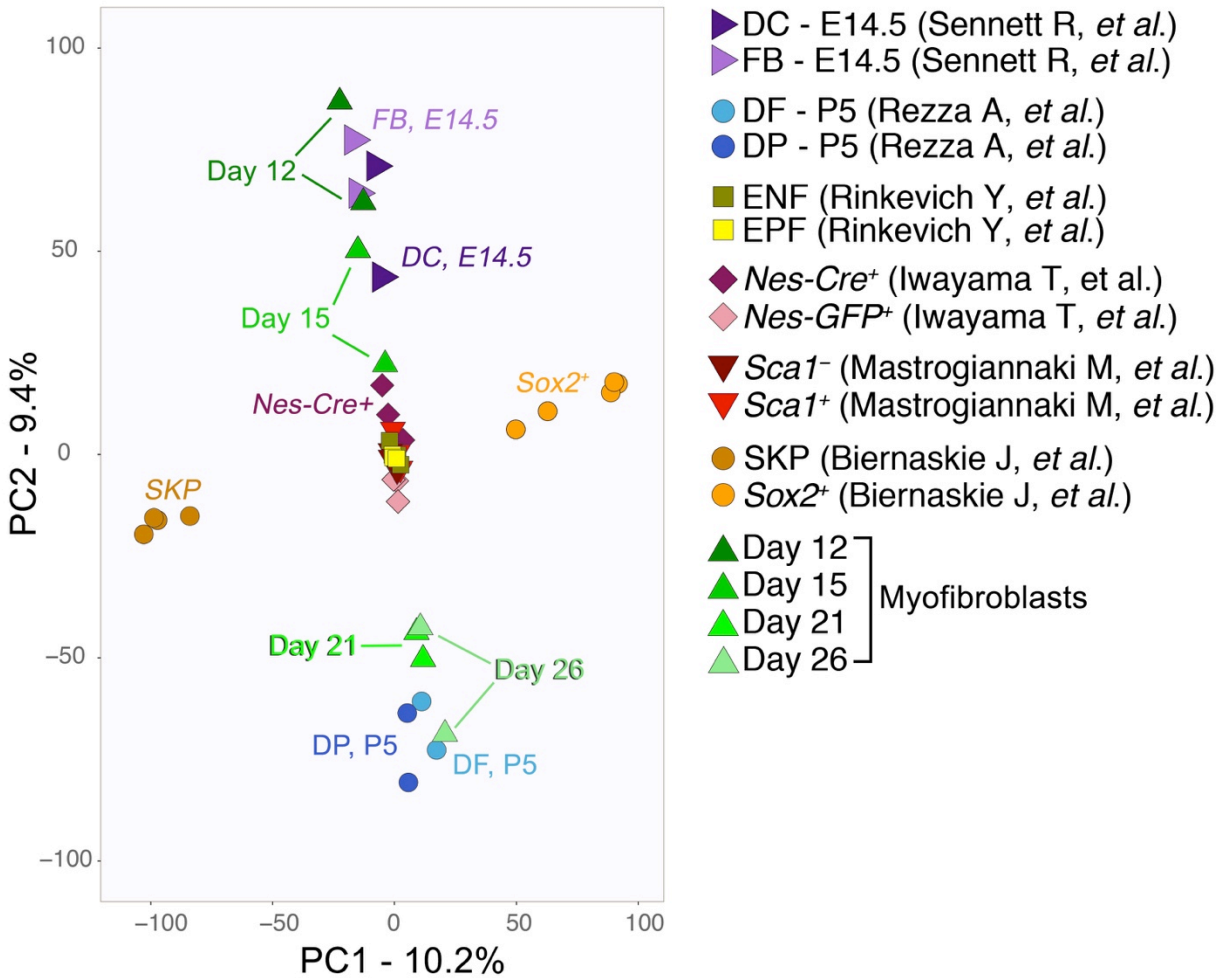


Fig. S15: Transcriptome-wide meta-analysis of wound myofibroblasts and dermal cells from unwounded skin. Transcriptome-wide comparison between myofibroblasts from days 12, 15, 21 and 26 (green triangles) and previously reported dermal cell populations (see “Meta-analyses” section of the Materials and methods for technical details). Analysis reveals that wound day 12 and 15 myofibroblasts cluster the closest to E14.5 dermal fibroblasts (DF) and dermal condensate (DC) cells (dark and light purple triangles), while wound day 21 and 26 myofibroblasts cluster near P5 dermal fibroblasts (DF) (light blue circles). Wound myofibroblasts at all time points are distinct from the reported primary passaged skin-derived precursor (SKP) cells (dark orange circles) and sorted *Sox2-GFP⁺;CD34^{neg}* (*Sox2⁺*) neonatal dermal cells (light orange circles).

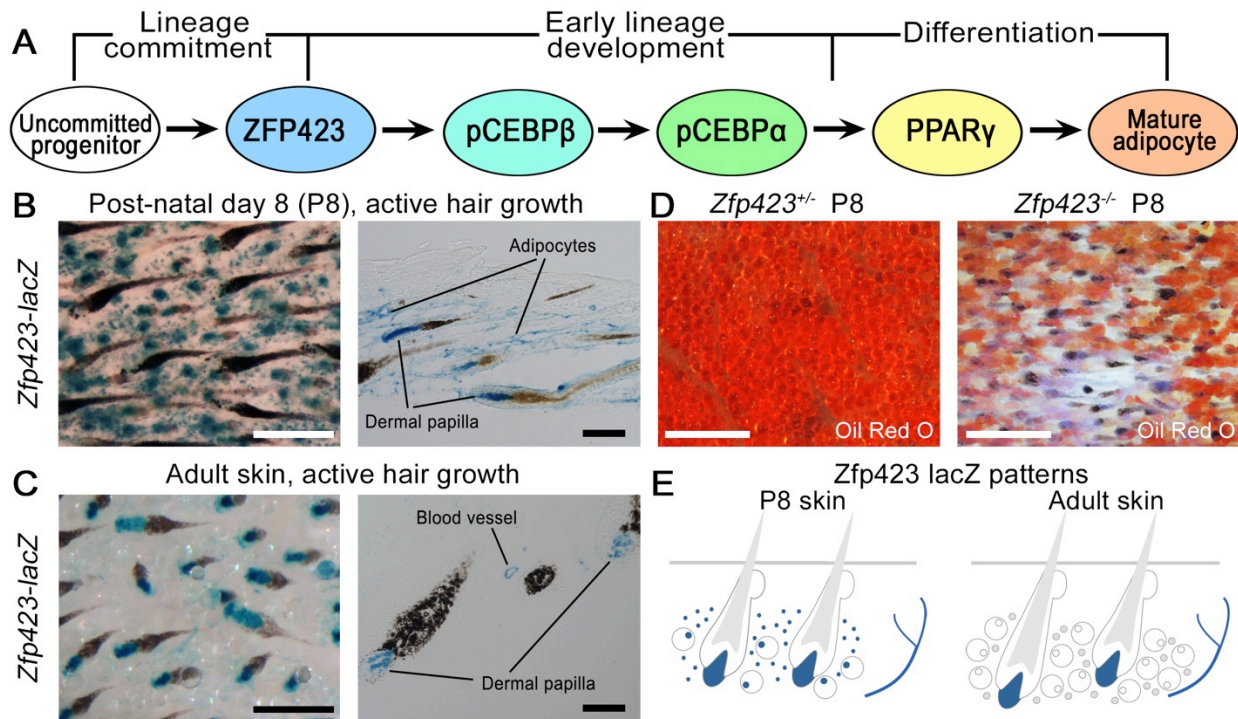


Fig. S16: Normal adipogenesis during skin development depends on Zfp423. (A) Schematic representation of the key signaling events in white adipose lineage development. (B, C) LacZ expression in *Zfp423-lacZ* reporter mice reveals transcriptional activation of *Zfp423* in dermal cells around hair follicles at post-natal day 8 (B), but not in adult skin during active hair growth (C). Note that the ZFP423 reporter is also active in dermal papillae and blood vessels. (D) At post-natal day 8, the cutaneous fat layer in dorsal skin of *Zfp423* null mice appears thinner than in control, but hair follicles develop normally. (E) Schematic representations depicting differences in ZFP423 reporter activity between developing and mature skin. **Views of underside of skin.** Scale bars in (B) to (D), 200 μ m.

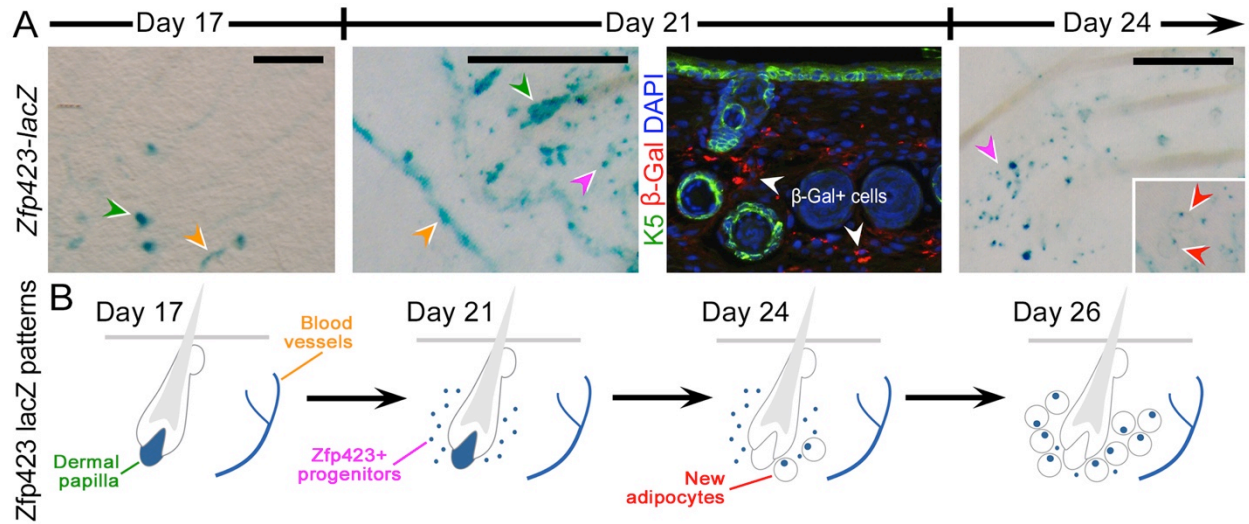


Fig. S17: Spatio-temporal patterns of *Zfp423* activity (*lacZ* expression) in the wounds of *Zfp423-lacZ* mice. (A) *Zfp423* activity (blue) was detected in dermal papilla of new hair follicles (green arrowheads), in blood vessels (orange arrowheads) and in dermal cells (purple arrowheads) surrounding new hair follicles starting at wound day 21. On wound day 24, new adipocytes (red arrowheads) also express *Zfp423* activity. Note that wound day 24 panel is an enlargement of fig. S18B (same sample). (B) Schematic depiction of *Zfp423* reporter patterns seen in regenerating wounds. Scale bars in (A), 200 μ m.

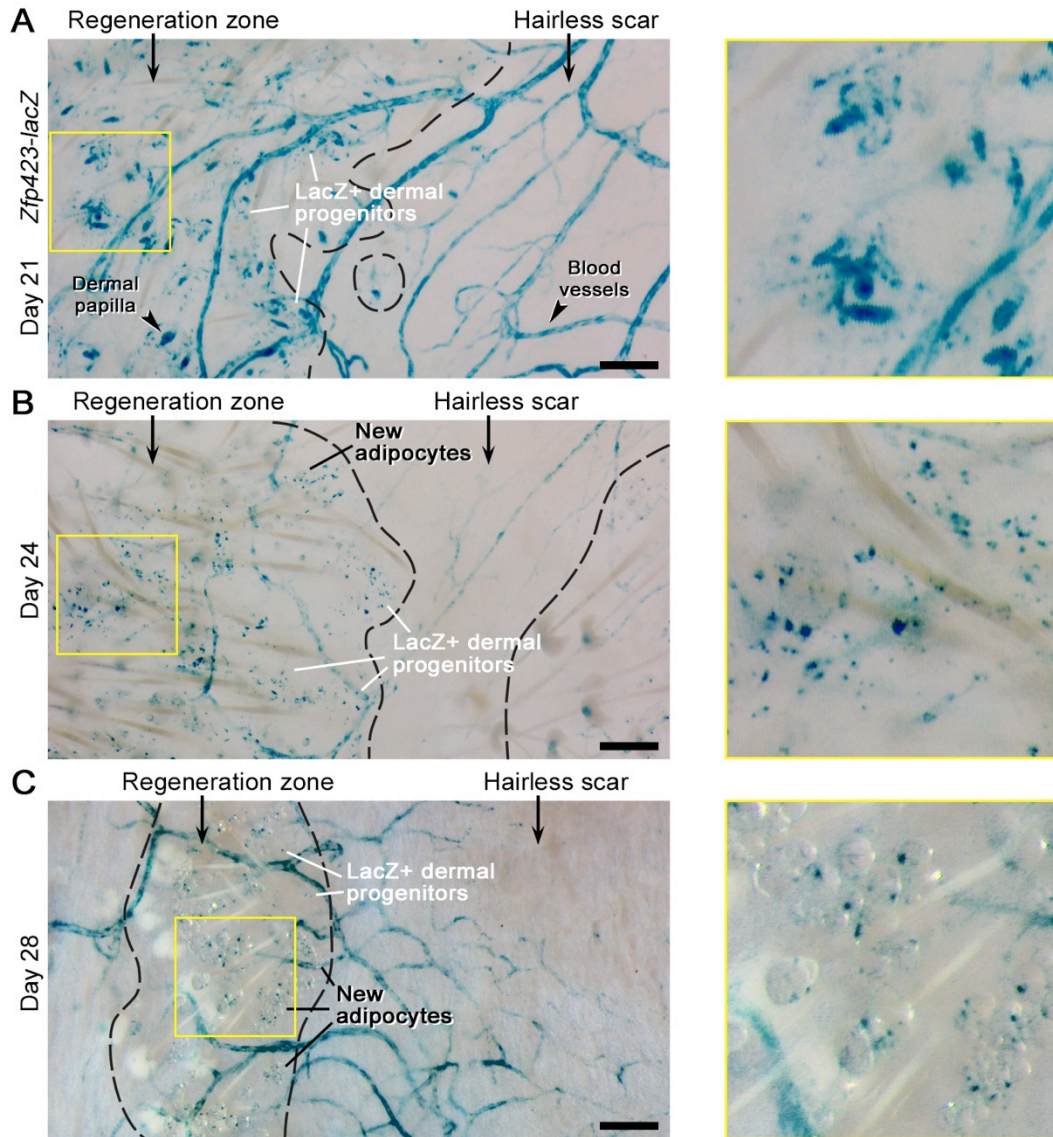


Fig. S18: Details of *Zfp423* activity (*lacZ* expression) in the wounds of *Zfp423-lacZ* mice. (A) Many *lacZ* positive cells start to appear in close proximity to new hair follicles on wound day 21. *LacZ* is also expressed on wound blood vessels, and by dermal papillae of virtually all new hair follicles (arrowheads). **(B)** On day 24, *lacZ* expression persists on dermal progenitors next to new hair follicles and on wound blood vessels. It turns off on dermal papillae of new hair follicles. Additionally, few newly differentiated new adipocytes express *lacZ*. **(C)** On wound day 28, the number of *lacZ* positive wound dermal progenitors sharply decreased, replaced by many *lacZ* positive mature adipocytes. Expression persists on wound blood vessels. **Views of underside of skin.** Scale bars in (A) to (C), 200 μ m.

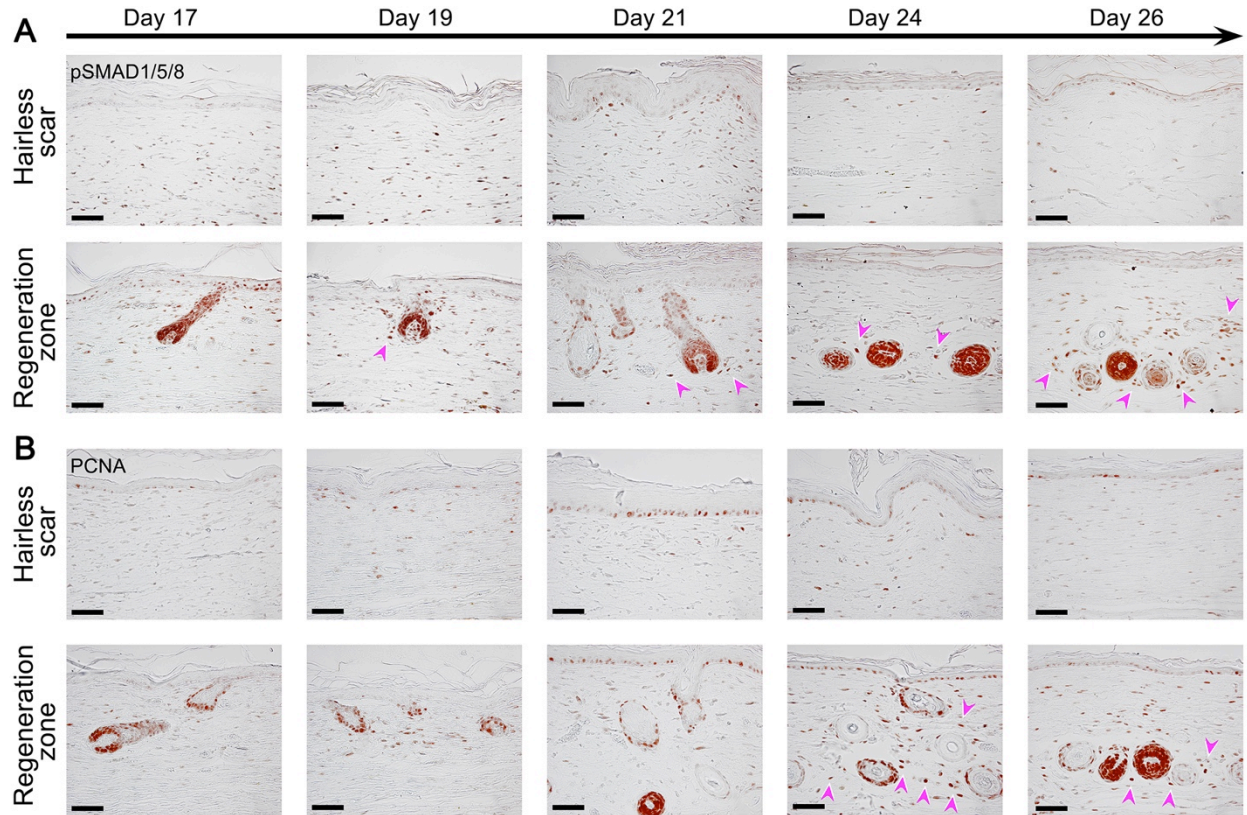


Fig. S19: Patterns of proliferation and BMP signaling during new fat regeneration. Large numbers of both pSMAD1/5/8 positive (**A**) and PCNA positive cells (**B**) appear in hair-bearing, but not hairless portions of the wound scar tissue on days 24 and 26 (purple arrowheads). Scale bars in (A) and (B), 50 μ m.

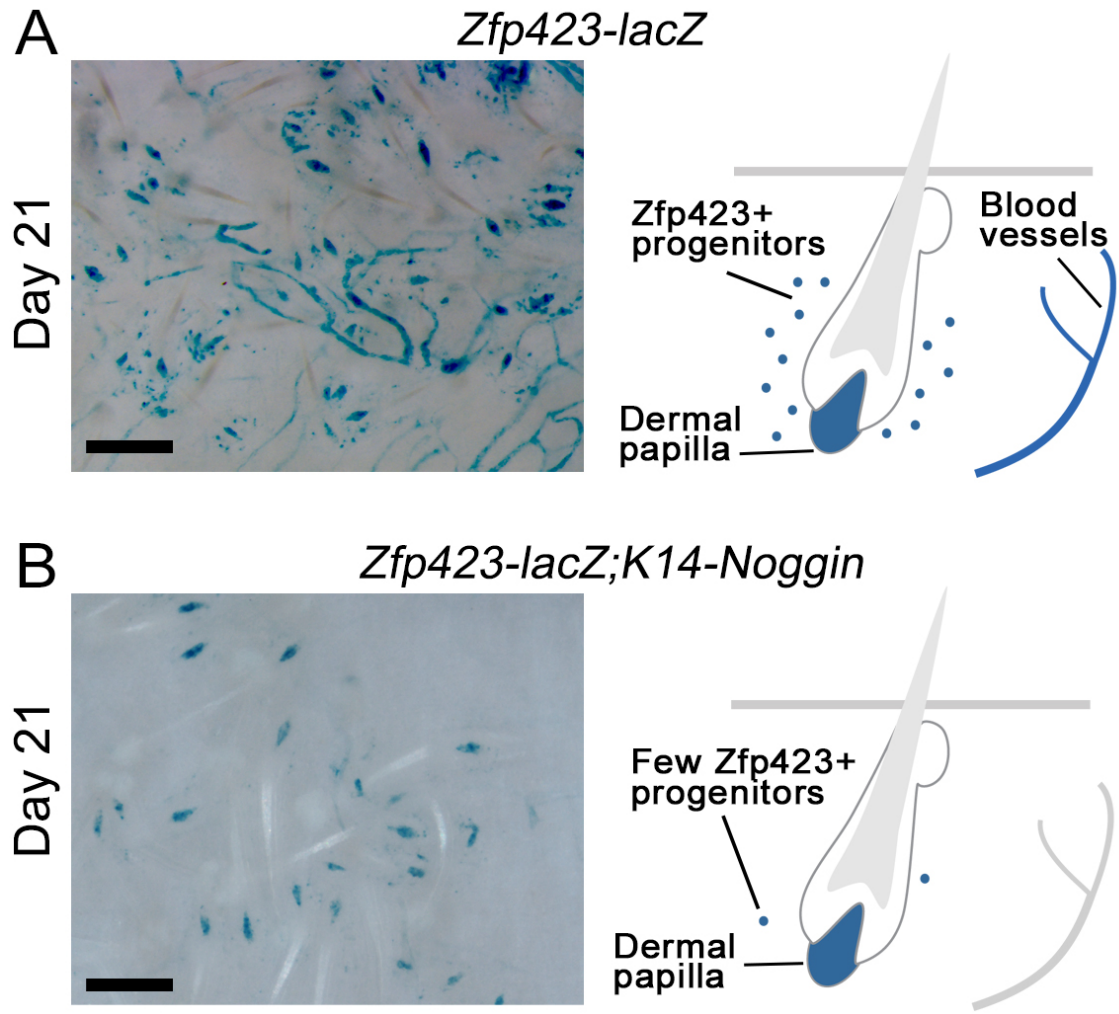


Fig. S20: BMP signaling is necessary for *Zfp423* reporter activation in regenerating wounds. (A, B) In *K14-Noggin* mice, which overexpress the soluble BMP antagonist noggin, *Zfp423* activity becomes significantly downregulated on day 21 in dermal wound cells surrounding new hair follicles, as well as in blood vessels. Scale bars in (A) and (B), 200 µm.

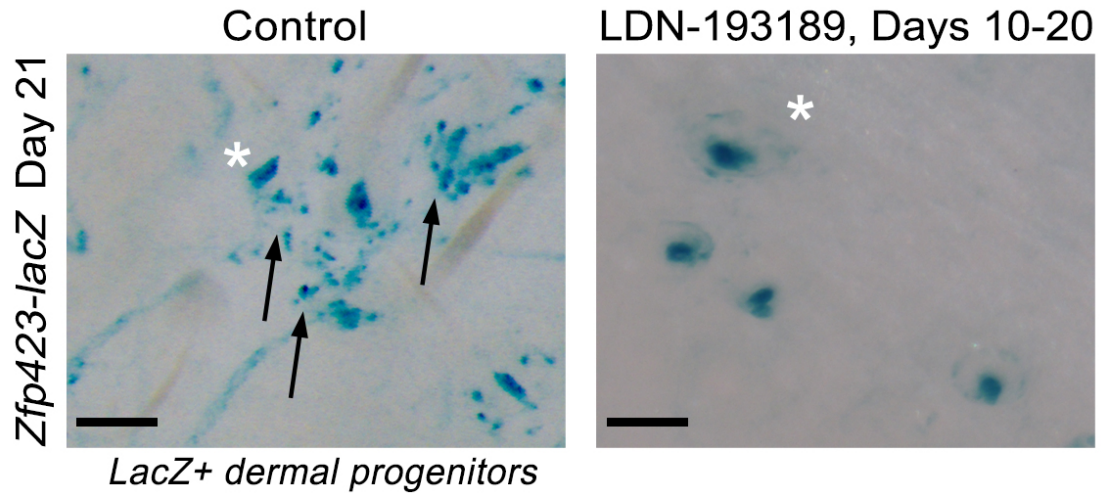


Fig. S21: BMP signaling is necessary for *Zfp423* reporter activation in wounds. Treatment with the BMP antagonist, LDN-193189 (2mg/kg), during wound healing significantly downregulated *Zfp423* activity on day 21 in dermal cells surrounding new hair follicles, and in blood vessels. Asterisk marks lacZ-positive dermal papillae of new hair follicles. Scale bars, 100 μ m.

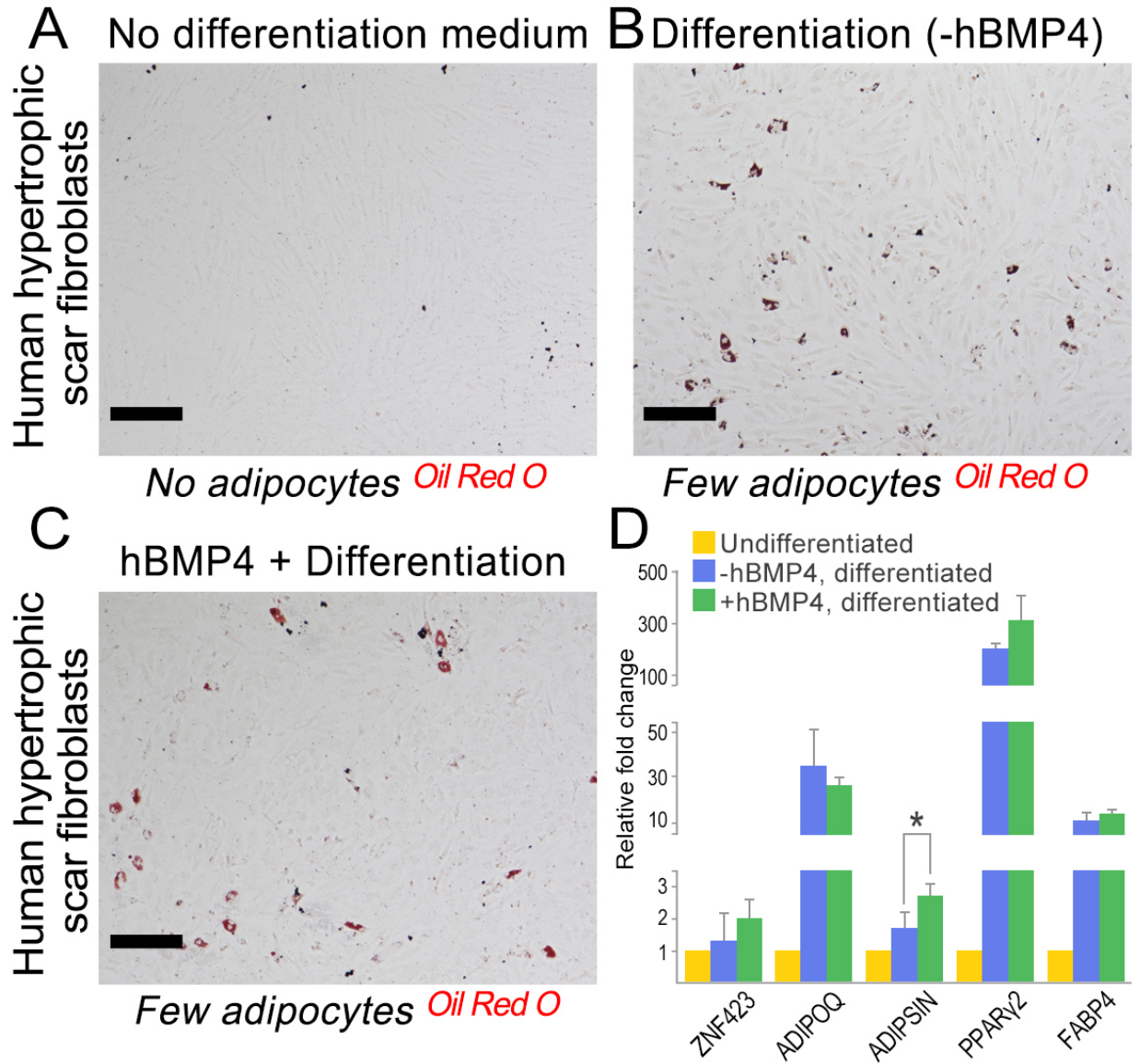


Fig. S22: Adipogenic differentiation of human hypertrophic scar fibroblasts. In vitro treatment of cells with hBMP4 prior to differentiation does not induce an increase in adipogenic potential in human hypertrophic scar fibroblasts (C) as compared to non-hBMP4 control (B). No adipocytes formed without differentiation media (A). Cells are stained for Oil Red O. (D) qRT-PCR against select adipogenic genes shows that only *ADIPSIN* becomes significantly upregulated following hBMP4 treatment (n=3). Scale bars in (A) to (C), 200 μ m. Values in the graphs are means \pm SEM. * $P = 0.0155$.

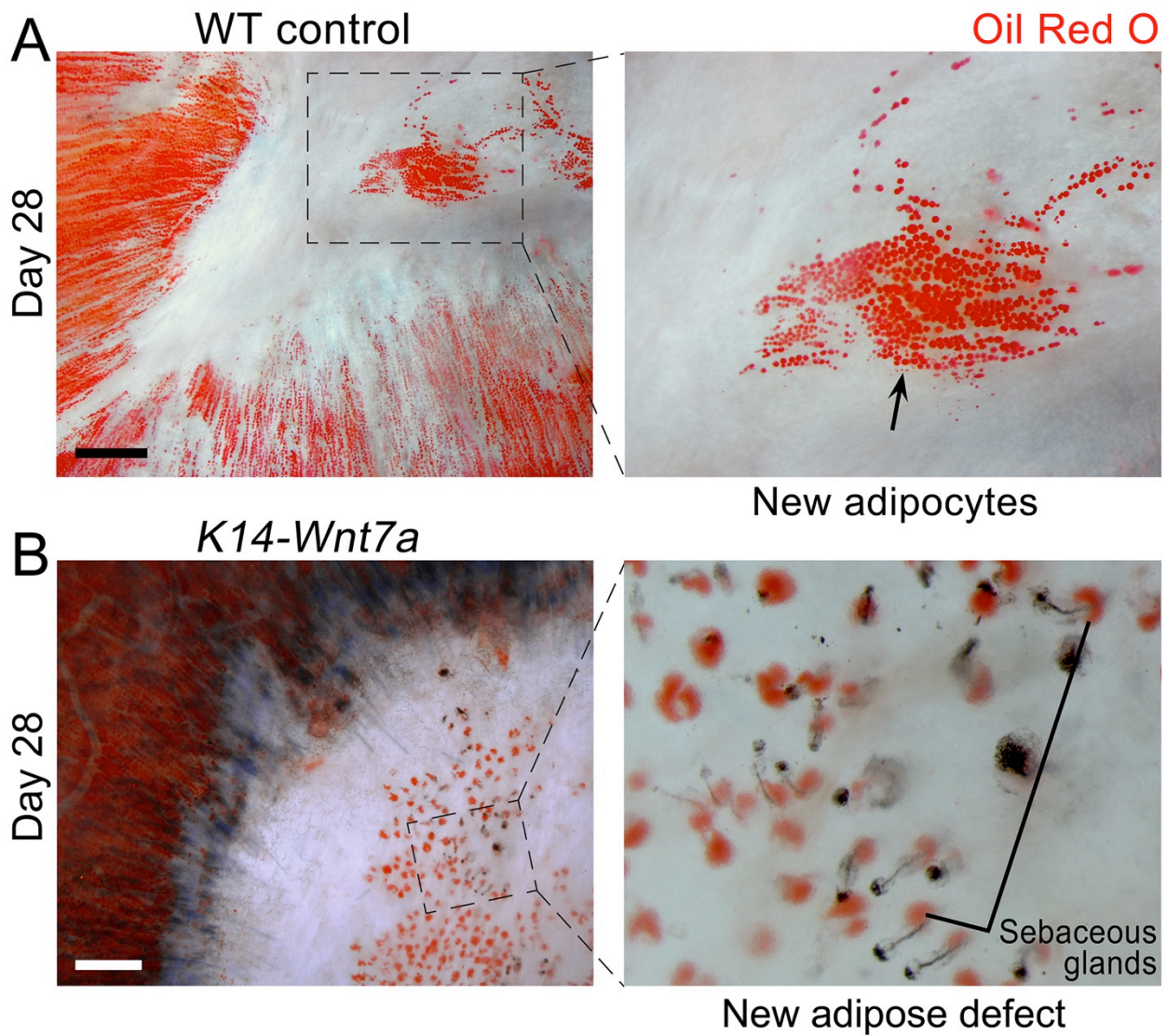


Fig. S23: Overexpression of WNT7a blocks adipocyte neogenesis in wounds. In contrast to WT control mice (A), in *K14-Wnt7a* mice overexpressing WNT7a (B), new adipocytes do not form after wounding despite formation of increased numbers of new hair follicles. Scale bars in (A) and (B), 1 mm.

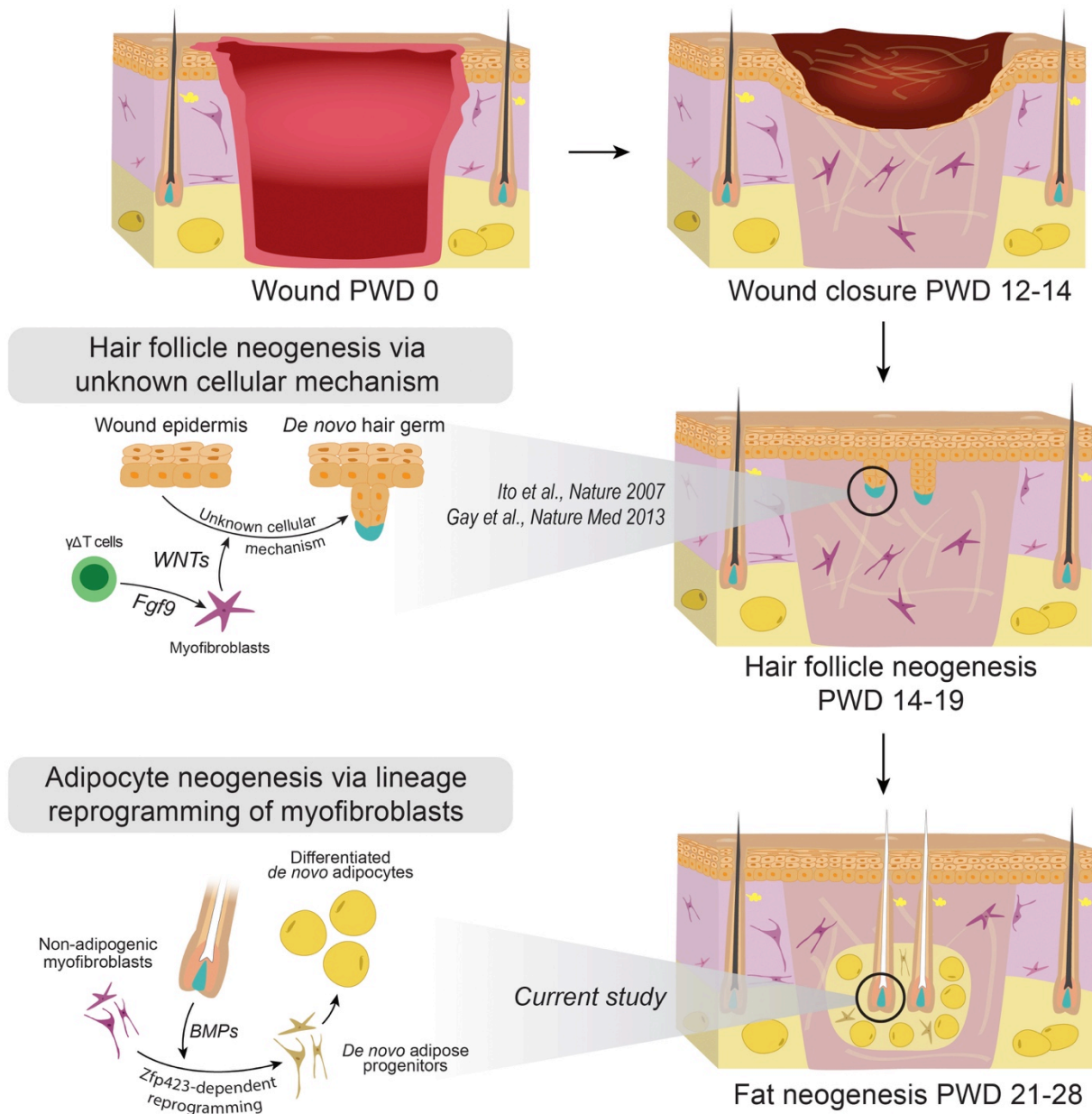


Fig. S24: Proposed model for wound induced hair follicle and fat regeneration in adult skin wounds. New hair follicles regenerate on days 14-19 via an Fgf9/WNT feedback loop-dependent signaling mechanisms. The cellular basis for hair regeneration (i.e. changes in cell lineage identity) remains to be established. Our current study reveals that new adipocytes regenerate on days 21-28 via BMP-ZFP423 driven lineage reprogramming of non-adipogenic wound myofibroblasts.

Supplementary Tables

Supplementary table S1: Mice used in the study.

| Transgenic mouse line | Adipocyte/hair follicle index | P value | Post-wounding day | N |
|---|-------------------------------|---------|-------------------|----|
| Experiment: Constitutive deletion of <i>Pparγ</i> in myofibroblasts | | | | |
| <i>SM22-Cre;Pparγ^{lox/lox}</i> (mutant) | 0.62 ± 0.2 | P<0.05 | Day 28 | 7 |
| <i>SM22-Cre;Pparγ^{lox/+}</i> (control) | 24.1 ± 6.8 | | Day 28 | 7 |
| Experiment: Inducible deletion of <i>Pparγ</i> in myofibroblasts | | | | |
| <i>SMA-CreERT2;Pparγ^{lox/lox}</i> (mutant) | 0.5 ± 0.07 | P<0.05 | Day 28 | 6 |
| <i>SMA-CreERT2;Pparγ^{lox/+}</i> (control) | 22.7 ± 5.1 | | Day 28 | 6 |
| Experiment: Whole-body deletion of <i>Zfp423</i> | | | | |
| <i>Zfp423</i> ^{-/-} (mutant) | 0.07 ± 0.06 | P<0.05 | Day 28 | 9 |
| <i>Zfp423</i> ^{+/-} (control) | 29.6 ± 5.4 | | Day 28 | 9 |
| Experiment: Skin specific over-expression of soluble BMP antagonist Noggin | | | | |
| <i>K14-Noggin</i> (mutant) | 0.2 ± 0.1 | P<0.05 | Day 28 | 10 |
| WT (control) | 30.6 ± 6.3 | | Day 28 | 10 |
| Experiment: Inducible deletion of BMP receptor <i>Bmpr1a</i> in myofibroblasts | | | | |
| <i>SMA-CreERT2;Bmpr1a^{lox/lox}</i> (mutant) | 0.38 ± 0.36 | P<0.05 | Day 28 | 6 |
| Tamoxifen treated control | 23.9 ± 1.5 | | Day 28 | 3 |
| Experiment: Pharmacological treatment of mice with LDN-193189 | | | | |
| WT (treated) | 0.58 ± 0.35 | P<0.05 | Day 28 | 7 |
| WT (vehicle control) | 5.8 ± 1.4 | | Day 28 | 4 |
| Experiment: Skin specific over-expression of soluble WNT ligand <i>Wnt7a</i> | | | | |
| <i>K14-Wnt7a</i> (mutant) | 0.6 ± 0.3 | P<0.05 | Day 28 | 6 |
| WT (control) | 28 ± 4.2 | | Day 28 | 6 |

Supplementary table S2: Primary human cells used in the study.

| ID | Gender | Ethnicity | Age (yrs.) | Source | Clinical History |
|---|--------|-------------|------------|--------|------------------|
| Wound healing pathology: Keloid scar | | | | | |
| K126 | Female | Caucasian | 62 | Breast | NA |
| K117 | Female | Caucasian | 30 | NA | NA |
| K120 | Female | A. American | NA | NA | NA |
| Wound healing pathology: Hypertrophic scar | | | | | |
| HS-1 | Female | Caucasian | 60 | Breast | NA |
| HS-2 | Female | Caucasian | 62 | Breast | Breast cancer |
| HS-3 | Female | Asian | 50 | Breast | Breast cancer |

Supplementary table S3: Mouse primers used in the study.

| Gene | Forward Primer (5' – 3') | Reverse Primer (5' – 3') |
|---------------|------------------------------|--------------------------|
| Mouse | | |
| <i>Gapdh</i> | GAAGGTGAAGGTCGGAGT | GAAGATGGTGATGGGATTTC |
| <i>Adipoq</i> | GCACTGGCAAGTTCTACTGCAA | GTAGGTGAAGAGAACGGCCTTGT |
| <i>Retn</i> | CTGTCCAGT CTA TCC TTG CAC AC | CAGAAGGCACAGCAGTCTTGA |
| <i>Pparg</i> | GTGCCAGTTTCGATCCGTAGA | GGCCAGCATCGTGTAGATGA |
| <i>Wnt2b</i> | AGAGTGCCAACACCAGTTCC | ACGAGGTCATTTTTTCGTTGG |
| <i>Sox9</i> | ACGGCTCCAGCAAGAACAAG | TTGTGCAGATGCGGGTACTG |
| <i>Zfp423</i> | TGGCCTGGGATTCCTCTGT | TTGTCGCACTGTTTCAGTTCTC |
| <i>Bmp4</i> | GCCCTGCAGTCCTTCGCTGG | CTGACGTGCTGGCCCTGGTG |
| <i>Lepr</i> | ACGTGGTGAAGCATCGTACT | GGCCATGAGAAGGTAAGGTT |
| <i>Wif1</i> | GATTTTCAGGAAAGCCCAACAAAGAA | GTTGGATCTGCCATGATGCCTTT |
| <i>Klf15</i> | CACCAAGAGCAGCCACCTCA | CGGGACACTGGTACGGCTTC |
| <i>Id1</i> | CGACTACATCAGGGACCTGCA | GAACACATGCCGCTCGG |
| <i>Dlk1</i> | AAGGACTGCCAGAAAAGGAC | GCAGAAATTGCCTGAGAAGC |

Supplementary table S4: Human primers used in the study.

| Gene | Forward Primer (5' – 3') | Reverse Primer (5' – 3') |
|----------------|--------------------------|--------------------------|
| Human | | |
| <i>ADIPOQ</i> | CCCAACATGCCCATTCGCTTT | ACAGCCCAGGAATGTTGCAGT |
| <i>ADIPSIN</i> | TGGAGGTGGGTGCTTGTAGTT | GGTGCAATCACAACACTCACTGC |
| <i>FABP4</i> | GTCATGAAAGGCGTCACTTCCAC | CAATGCGAACTTCAGTCCAGGTC |
| <i>PPARG2</i> | GCAGGAGATCACAGAGTATGCCA | TCAAGGAGGCCAGCATTGTGT |
| <i>RPS18</i> | TGCAGAAATCCACGCCAGTACA | ATCTTCTTCAGTCGCTCCAGGTC |
| <i>ZNF423</i> | CCAAATCCACGTTGCCAACCA | TGCTCAATGAGGTGACAGAGGAG |

References and Notes

1. D. Gay, O. Kwon, Z. Zhang, M. Spata, M. V. Plikus, P. D. Holler, M. Ito, Z. Yang, E. Treffeisen, C. D. Kim, A. Nace, X. Zhang, S. Baratono, F. Wang, D. M. Ornitz, S. E. Millar, G. Cotsarelis, Fgf9 from dermal $\gamma\delta$ T cells induces hair follicle neogenesis after wounding. *Nat. Med.* **19**, 916–923 (2013). [doi:10.1038/nm.3181](https://doi.org/10.1038/nm.3181) [Medline](#)
2. M. Ito, Z. Yang, T. Andl, C. Cui, N. Kim, S. E. Millar, G. Cotsarelis, Wnt-dependent de novo hair follicle regeneration in adult mouse skin after wounding. *Nature* **447**, 316–320 (2007). [doi:10.1038/nature05766](https://doi.org/10.1038/nature05766) [Medline](#)
3. A. W. Seifert, S. G. Kiama, M. G. Seifert, J. R. Goheen, T. M. Palmer, M. Maden, Skin shedding and tissue regeneration in African spiny mice (*Acomys*). *Nature* **489**, 561–565 (2012). [doi:10.1038/nature11499](https://doi.org/10.1038/nature11499) [Medline](#)
4. X. Wang, T.-C. Hsi, C. F. Guerrero-Juarez, K. Pham, K. Cho, C. D. McCusker, E. S. Monuki, K. W. Y. Cho, D. L. Gay, M. V. Plikus, Principles and mechanisms of regeneration in the mouse model for wound-induced hair follicle neogenesis. *Regeneration* **2**, 169–181 (2015). [doi:10.1002/reg2.38](https://doi.org/10.1002/reg2.38) [Medline](#)
5. C. Breedis, Regeneration of hair follicles and sebaceous glands from the epithelium of scars in the rabbit. *Cancer Res.* **14**, 575–579 (1954). [Medline](#)
6. R. E. Billingham, P. S. Russell, Incomplete wound contracture and the phenomenon of hair neogenesis in rabbits' skin. *Nature* **177**, 791–792 (1956). [doi:10.1038/177791b0](https://doi.org/10.1038/177791b0) [Medline](#)
7. R. R. Banerjee, S. M. Rangwala, J. S. Shapiro, A. S. Rich, B. Rhoades, Y. Qi, J. Wang, M. W. Rajala, A. Poci, P. E. Scherer, C. M. Steppan, R. S. Ahima, S. Obici, L. Rossetti, M. A. Lazar, Regulation of fasted blood glucose by resistin. *Science* **303**, 1195–1198 (2004). [doi:10.1126/science.1092341](https://doi.org/10.1126/science.1092341) [Medline](#)
8. J. Ishibashi, Z. Firtina, S. Rajakumari, K. H. Wood, H. M. Conroe, D. J. Steger, P. Seale, An Evi1-C/EBP β complex controls peroxisome proliferator-activated receptor γ 2 gene expression to initiate white fat cell differentiation. *Mol. Cell. Biol.* **32**, 2289–2299 (2012). [doi:10.1128/MCB.06529-11](https://doi.org/10.1128/MCB.06529-11) [Medline](#)
9. R. K. Gupta, Z. Arany, P. Seale, R. J. Mepani, L. Ye, H. M. Conroe, Y. A. Roby, H. Kulaga, R. R. Reed, B. M. Spiegelman, Transcriptional control of preadipocyte determination by Zfp423. *Nature* **464**, 619–623 (2010). [doi:10.1038/nature08816](https://doi.org/10.1038/nature08816) [Medline](#)
10. S. Kang, P. Akerblad, R. Kiviranta, R. K. Gupta, S. Kajimura, M. J. Griffin, J. Min, R. Baron, E. D. Rosen, Regulation of early adipose commitment by Zfp521. *PLOS Biol.* **10**, e1001433 (2012). [doi:10.1371/journal.pbio.1001433](https://doi.org/10.1371/journal.pbio.1001433) [Medline](#)
11. W. Tang, D. Zeve, J. M. Suh, D. Bosnakovski, M. Kyba, R. E. Hammer, M. D. Tallquist, J. M. Graff, White fat progenitor cells reside in the adipose vasculature. *Science* **322**, 583–586 (2008). [doi:10.1126/science.1156232](https://doi.org/10.1126/science.1156232) [Medline](#)
12. W. A. Alcaraz, D. A. Gold, E. Raponi, P. M. Gent, D. Concepcion, B. A. Hamilton, Zfp423 controls proliferation and differentiation of neural precursors in cerebellar vermis formation. *Proc. Natl. Acad. Sci. U.S.A.* **103**, 19424–19429 (2006). [doi:10.1073/pnas.0609184103](https://doi.org/10.1073/pnas.0609184103) [Medline](#)

13. A. Hammarstedt, S. Hedjazifar, L. Jenndahl, S. Gogg, J. Grünberg, B. Gustafson, E. Klimcakova, V. Stich, D. Langin, M. Laakso, U. Smith, WISP2 regulates preadipocyte commitment and PPAR γ activation by BMP4. *Proc. Natl. Acad. Sci. U.S.A.* **110**, 2563–2568 (2013). [doi:10.1073/pnas.1211255110](https://doi.org/10.1073/pnas.1211255110) [Medline](#)
14. H. Kulesa, G. Turk, B. L. Hogan, Inhibition of Bmp signaling affects growth and differentiation in the anagen hair follicle. *EMBO J.* **19**, 6664–6674 (2000). [doi:10.1093/emboj/19.24.6664](https://doi.org/10.1093/emboj/19.24.6664) [Medline](#)
15. R. R. Driskell, B. M. Lichtenberger, E. Hoste, K. Kretzschmar, B. D. Simons, M. Charalambous, S. R. Ferron, Y. Herault, G. Pavlovic, A. C. Ferguson-Smith, F. M. Watt, Distinct fibroblast lineages determine dermal architecture in skin development and repair. *Nature* **504**, 277–281 (2013). [doi:10.1038/nature12783](https://doi.org/10.1038/nature12783) [Medline](#)
16. S. Dulauroy, S. E. Di Carlo, F. Langa, G. Eberl, L. Peduto, Lineage tracing and genetic ablation of ADAM12⁺ perivascular cells identify a major source of profibrotic cells during acute tissue injury. *Nat. Med.* **18**, 1262–1270 (2012). [doi:10.1038/nm.2848](https://doi.org/10.1038/nm.2848) [Medline](#)
17. H. Suga, R. C. Rennert, M. Rodrigues, M. Sorkin, J. P. Glotzbach, M. Januszyk, T. Fujiwara, M. T. Longaker, G. C. Gurtner, Tracking the elusive fibrocyte: Identification and characterization of collagen-producing hematopoietic lineage cells during murine wound healing. *Stem Cells* **32**, 1347–1360 (2014). [doi:10.1002/stem.1648](https://doi.org/10.1002/stem.1648) [Medline](#)
18. Y. Rinkevich, G. G. Walmsley, M. S. Hu, Z. N. Maan, A. M. Newman, M. Drukker, M. Januszyk, G. W. Krampitz, G. C. Gurtner, H. P. Lorenz, I. L. Weissman, M. T. Longaker, Identification and isolation of a dermal lineage with intrinsic fibrogenic potential. *Science* **348**, aaa2151 (2015). [doi:10.1126/science.aaa2151](https://doi.org/10.1126/science.aaa2151) [Medline](#)
19. M. V. Plikus, C. F. Guerrero-Juarez, E. Treffeisen, D. L. Gay, Epigenetic control of skin and hair regeneration after wounding. *Exp. Dermatol.* **24**, 167–170 (2015). [doi:10.1111/exd.12488](https://doi.org/10.1111/exd.12488) [Medline](#)
20. J. A. Lehoczy, B. Robert, C. J. Tabin, Mouse digit tip regeneration is mediated by fate-restricted progenitor cells. *Proc. Natl. Acad. Sci. U.S.A.* **108**, 20609–20614 (2011). [doi:10.1073/pnas.1118017108](https://doi.org/10.1073/pnas.1118017108) [Medline](#)
21. Y. Rinkevich, P. Lindau, H. Ueno, M. T. Longaker, I. L. Weissman, Germ-layer and lineage-restricted stem/progenitors regenerate the mouse digit tip. *Nature* **476**, 409–413 (2011). [doi:10.1038/nature10346](https://doi.org/10.1038/nature10346) [Medline](#)
22. T. H. Leung, E. R. Snyder, Y. Liu, J. Wang, S. K. Kim, A cellular, molecular, and pharmacological basis for appendage regeneration in mice. *Genes Dev.* **29**, 2097–2107 (2015). [doi:10.1101/gad.267724.115](https://doi.org/10.1101/gad.267724.115) [Medline](#)
23. Y. S. Lee, T. Hsu, W.-C. Chiu, H. Sarkozy, D. A. Kulber, A. Choi, E. W. Kim, P. D. Benya, T.-L. Tuan, Keloid-derived, plasma/fibrin-based skin equivalents generate de novo dermal and epidermal pathology of keloid fibrosis in a mouse model. *Wound Repair Regen.* **24**, 302–316 (2016). [doi:10.1111/wrr.12397](https://doi.org/10.1111/wrr.12397) [Medline](#)
24. M. Vangipuram, D. Ting, S. Kim, R. Diaz, B. Schüle, Skin punch biopsy explant culture for derivation of primary human fibroblasts. *J. Vis. Exp.* **2013**, e3779 (2013). [Medline](#)

25. M. P. Philpott, M. R. Green, T. Kealey, Human hair growth in vitro. *J. Cell Sci.* **97**, 463–471 (1990). [Medline](#)
26. S. Picelli, Å. K. Björklund, O. R. Faridani, S. Sagasser, G. Winberg, R. Sandberg, Smart-seq2 for sensitive full-length transcriptome profiling in single cells. *Nat. Methods* **10**, 1096–1098 (2013). [doi:10.1038/nmeth.2639](https://doi.org/10.1038/nmeth.2639) [Medline](#)
27. S. Picelli, O. R. Faridani, Å. K. Björklund, G. Winberg, S. Sagasser, R. Sandberg, Full-length RNA-seq from single cells using Smart-seq2. *Nat. Protoc.* **9**, 171–181 (2014). [doi:10.1038/nprot.2014.006](https://doi.org/10.1038/nprot.2014.006) [Medline](#)
28. B. Li, C. N. Dewey, RSEM: Accurate transcript quantification from RNA-Seq data with or without a reference genome. *BMC Bioinformatics* **12**, 323 (2011). [doi:10.1186/1471-2105-12-323](https://doi.org/10.1186/1471-2105-12-323) [Medline](#)
29. A. Conesa, M. J. Nueda, A. Ferrer, M. Talón, maSigPro: A method to identify significantly differential expression profiles in time-course microarray experiments. *Bioinformatics* **22**, 1096–1102 (2006). [doi:10.1093/bioinformatics/btl056](https://doi.org/10.1093/bioinformatics/btl056) [Medline](#)
30. M. J. Nueda, S. Tarazona, A. Conesa, Next maSigPro: Updating maSigPro bioconductor package for RNA-seq time series. *Bioinformatics* **30**, 2598–2602 (2014). [doi:10.1093/bioinformatics/btu333](https://doi.org/10.1093/bioinformatics/btu333) [Medline](#)
31. J. Biernaskie, M. Paris, O. Morozova, B. M. Fagan, M. Marra, L. Pevny, F. D. Miller, SKPs derive from hair follicle precursors and exhibit properties of adult dermal stem cells. *Cell Stem Cell* **5**, 610–623 (2009). [doi:10.1016/j.stem.2009.10.019](https://doi.org/10.1016/j.stem.2009.10.019) [Medline](#)
32. T. Iwayama, C. Steele, L. Yao, M. G. Dozmorov, D. Karamichos, J. D. Wren, L. E. Olson, PDGFR α signaling drives adipose tissue fibrosis by targeting progenitor cell plasticity. *Genes Dev.* **29**, 1106–1119 (2015). [doi:10.1101/gad.260554.115](https://doi.org/10.1101/gad.260554.115) [Medline](#)
33. R. Sennett, Z. Wang, A. Rezza, L. Grisanti, N. Roitershtein, C. Sicchio, K. W. Mok, N. J. Heitman, C. Clavel, A. Ma'ayan, M. Rendl, An integrated transcriptome atlas of embryonic hair follicle progenitors, their niche, and the developing skin. *Dev. Cell* **34**, 577–591 (2015). [doi:10.1016/j.devcel.2015.06.023](https://doi.org/10.1016/j.devcel.2015.06.023) [Medline](#)
34. A. Rezza, Z. Wang, R. Sennett, W. Qiao, D. Wang, N. Heitman, K. W. Mok, C. Clavel, R. Yi, P. Zandstra, A. Ma'ayan, M. Rendl, Signaling networks among stem cell precursors, transit-amplifying progenitors, and their niche in developing hair follicles. *Cell Reports* **14**, 3001–3018 (2016). [doi:10.1016/j.celrep.2016.02.078](https://doi.org/10.1016/j.celrep.2016.02.078) [Medline](#)
35. M. Mastrogiannaki, B. M. Lichtenberger, A. Reimer, C. A. Collins, R. R. Driskell, F. M. Watt, β -catenin stabilization in skin fibroblasts causes fibrotic lesions by preventing adipocyte differentiation of the reticular dermis. *J. Invest. Dermatol.* **136**, 1130–1142 (2016). [doi:10.1016/j.jid.2016.01.036](https://doi.org/10.1016/j.jid.2016.01.036) [Medline](#)
36. J. M. Miano, P. Cserjesi, K. L. Ligon, M. Periasamy, E. N. Olson, Smooth muscle myosin heavy chain exclusively marks the smooth muscle lineage during mouse embryogenesis. *Circ. Res.* **75**, 803–812 (1994). [doi:10.1161/01.RES.75.5.803](https://doi.org/10.1161/01.RES.75.5.803) [Medline](#)
37. B. Hinz, D. Mastrangelo, C. E. Iselin, C. Chaponnier, G. Gabbiani, Mechanical tension controls granulation tissue contractile activity and myofibroblast differentiation. *Am. J. Pathol.* **159**, 1009–1020 (2001). [doi:10.1016/S0002-9440\(10\)61776-2](https://doi.org/10.1016/S0002-9440(10)61776-2) [Medline](#)

38. A. Wirth, Z. Benyó, M. Lukasova, B. Leutgeb, N. Wettschureck, S. Gorbey, P. Örsy, B. Horváth, C. Maser-Gluth, E. Greiner, B. Lemmer, G. Schütz, J. S. Gutkind, S. Offermanns, G12-G13–LARG–mediated signaling in vascular smooth muscle is required for salt-induced hypertension. *Nat. Med.* **14**, 64–68 (2008). [doi:10.1038/nm1666](https://doi.org/10.1038/nm1666) [Medline](#)
39. S. Amini-Nik, D. Glancy, C. Boimer, H. Whetstone, C. Keller, B. A. Alman, Pax7 expressing cells contribute to dermal wound repair, regulating scar size through a β -catenin mediated process. *Stem Cells* **29**, 1371–1379 (2011). [Medline](#)
40. C. Lepper, C. M. Fan, Inducible lineage tracing of Pax7-descendant cells reveals embryonic origin of adult satellite cells. *Genesis* **48**, 424–436 (2010). [doi:10.1002/dvg.20630](https://doi.org/10.1002/dvg.20630) [Medline](#)
41. C. Lepper, S. J. Conway, C. M. Fan, Adult satellite cells and embryonic muscle progenitors have distinct genetic requirements. *Nature* **460**, 627–631 (2009). [doi:10.1038/nature08209](https://doi.org/10.1038/nature08209) [Medline](#)
42. G. S. Kaushal, E. Rognoni, B. M. Lichtenberger, R. R. Driskell, K. Kretschmar, E. Hoste, F. M. Watt, Fate of prominin-1 expressing dermal papilla cells during homeostasis, wound healing and Wnt activation. *J. Invest. Dermatol.* **135**, 2926–2934 (2015). [doi:10.1038/jid.2015.319](https://doi.org/10.1038/jid.2015.319) [Medline](#)
43. L. Zhu, P. Gibson, D. S. Currle, Y. Tong, R. J. Richardson, I. T. Bayazitov, H. Poppleton, S. Zakharenko, D. W. Ellison, R. J. Gilbertson, Prominin 1 marks intestinal stem cells that are susceptible to neoplastic transformation. *Nature* **457**, 603–607 (2009). [doi:10.1038/nature07589](https://doi.org/10.1038/nature07589) [Medline](#)
44. R. R. Driskell, A. Giangreco, K. B. Jensen, K. W. Mulder, F. M. Watt, Sox2-positive dermal papilla cells specify hair follicle type in mammalian epidermis. *Development* **136**, 2815–2823 (2009). [doi:10.1242/dev.038620](https://doi.org/10.1242/dev.038620) [Medline](#)
45. Y. Zheng, X. Du, W. Wang, M. Boucher, S. Parimoo, K. Stenn, Organogenesis from dissociated cells: Generation of mature cycling hair follicles from skin-derived cells. *J. Invest. Dermatol.* **124**, 867–876 (2005). [doi:10.1111/j.0022-202X.2005.23716.x](https://doi.org/10.1111/j.0022-202X.2005.23716.x) [Medline](#)
46. K. Wojciechowicz, E. Markiewicz, C. A. Jahoda, C/EBP α identifies differentiating preadipocytes around hair follicles in foetal and neonatal rat and mouse skin. *Exp. Dermatol.* **17**, 675–680 (2008). [doi:10.1111/j.1600-0625.2007.00689.x](https://doi.org/10.1111/j.1600-0625.2007.00689.x) [Medline](#)
47. A. Peláez-García, R. Barderas, R. Batlle, R. Viñas-Castells, R. A. Bartolomé, S. Torres, M. Mendes, M. Lopez-Lucendo, R. Mazzolini, F. Bonilla, A. García de Herreros, J. I. Casal, A proteomic analysis reveals that Snail regulates the expression of the nuclear orphan receptor Nuclear Receptor Subfamily 2 Group F Member 6 (Nr2f6) and interleukin 17 (IL-17) to inhibit adipocyte differentiation. *Mol. Cell. Proteomics* **14**, 303–315 (2015). [doi:10.1074/mcp.M114.045328](https://doi.org/10.1074/mcp.M114.045328) [Medline](#)
48. R. L. Landsberg, J. E. Sero, P. S. Danielian, T. L. Yuan, E. Y. Lee, J. A. Lees, The role of E2F4 in adipogenesis is independent of its cell cycle regulatory activity. *Proc. Natl. Acad. Sci. U.S.A.* **100**, 2456–2461 (2003). [doi:10.1073/pnas.0138064100](https://doi.org/10.1073/pnas.0138064100) [Medline](#)
49. U. J. Yun, N.-J. Song, D. K. Yang, S.-M. Kwon, K. Kim, S. Kim, D.-G. Jo, W. J. Park, K. W. Park, H. Kang, miR-195a inhibits adipocyte differentiation by targeting the

- preadipogenic determinant Zfp423. *J. Cell. Biochem.* **116**, 2589–2597 (2015).
[doi:10.1002/jcb.25204](https://doi.org/10.1002/jcb.25204) [Medline](#)
50. L. J. Zhang, C. F. Guerrero-Juarez, T. Hata, S. P. Bapat, R. Ramos, M. V. Plikus, R. L. Gallo, Dermal adipocytes protect against invasive *Staphylococcus aureus* skin infection. *Science* **347**, 67–71 (2015). [doi:10.1126/science.1260972](https://doi.org/10.1126/science.1260972) [Medline](#)
51. W. N. Addison, M. M. Fu, H. X. Yang, Z. Lin, K. Nagano, F. Gori, R. Baron, Direct transcriptional repression of Zfp423 by Zfp521 mediates a bone morphogenic protein-dependent osteoblast versus adipocyte lineage commitment switch. *Mol. Cell. Biol.* **34**, 3076–3085 (2014). [doi:10.1128/MCB.00185-14](https://doi.org/10.1128/MCB.00185-14) [Medline](#)
52. R. K. Gupta, R. J. Mepani, S. Kleiner, J. C. Lo, M. J. Khandekar, P. Cohen, A. Frontini, D. C. Bhowmick, L. Ye, S. Cinti, B. M. Spiegelman, Zfp423 expression identifies committed preadipocytes and localizes to adipose endothelial and perivascular cells. *Cell Metab.* **15**, 230–239 (2012). [doi:10.1016/j.cmet.2012.01.010](https://doi.org/10.1016/j.cmet.2012.01.010) [Medline](#)
53. X. Ma, H. Zhang, L. Yuan, H. Jing, P. Thacker, D. Li, CREBL2, interacting with CREB, induces adipogenesis in 3T3-L1 adipocytes. *Biochem. J.* **439**, 27–38 (2011).
[doi:10.1042/BJ20101475](https://doi.org/10.1042/BJ20101475) [Medline](#)
54. P. Gao, Y. Zhang, Y. Liu, J. Chen, C. Zong, C. Yu, S. Cui, W. Gao, D. Qin, W. Sun, X. Li, X. Wang, Signal transducer and activator of transcription 5B (STAT5B) modulates adipocyte differentiation via MOF. *Cell. Signal.* **27**, 2434–2443 (2015).
[doi:10.1016/j.cellsig.2015.09.010](https://doi.org/10.1016/j.cellsig.2015.09.010) [Medline](#)
55. H. Wakao, R. Wakao, A. Oda, H. Fujita, Constitutively active Stat5A and Stat5B promote adipogenesis. *Environ. Health Prev. Med.* **16**, 247–252 (2011). [doi:10.1007/s12199-010-0193-7](https://doi.org/10.1007/s12199-010-0193-7) [Medline](#)
56. J. M. Stephens, R. F. Morrison, Z. Wu, S. R. Farmer, PPAR γ ligand-dependent induction of STAT1, STAT5A, and STAT5B during adipogenesis. *Biochem. Biophys. Res. Commun.* **262**, 216–222 (1999). [doi:10.1006/bbrc.1999.0889](https://doi.org/10.1006/bbrc.1999.0889) [Medline](#)
57. S. Lee, H. Choi, B. S. Han, W. K. Kim, S. C. Lee, K.-J. Oh, K.-H. Bae, c-Jun regulates adipocyte differentiation via the KLF15-mediated mode. *Biochem. Biophys. Res. Commun.* **469**, 552–558 (2016). [doi:10.1016/j.bbrc.2015.12.035](https://doi.org/10.1016/j.bbrc.2015.12.035) [Medline](#)
58. T. Mori, H. Sakaue, H. Iguchi, H. Gomi, Y. Okada, Y. Takashima, K. Nakamura, T. Nakamura, T. Yamauchi, N. Kubota, T. Kadowaki, Y. Matsuki, W. Ogawa, R. Hiramatsu, M. Kasuga, Role of Krüppel-like factor 15 (KLF15) in transcriptional regulation of adipogenesis. *J. Biol. Chem.* **280**, 12867–12875 (2005).
[doi:10.1074/jbc.M410515200](https://doi.org/10.1074/jbc.M410515200) [Medline](#)
59. Y. Mori-Akiyama, H. Akiyama, D. H. Rowitch, B. de Crombrughe, Sox9 is required for determination of the chondrogenic cell lineage in the cranial neural crest. *Proc. Natl. Acad. Sci. U.S.A.* **100**, 9360–9365 (2003). [doi:10.1073/pnas.1631288100](https://doi.org/10.1073/pnas.1631288100) [Medline](#)
60. V. Lefebvre, P. Li, B. de Crombrughe, A new long form of Sox5 (L-Sox5), Sox6 and Sox9 are coexpressed in chondrogenesis and cooperatively activate the type II collagen gene. *EMBO J.* **17**, 5718–5733 (1998). [doi:10.1093/emboj/17.19.5718](https://doi.org/10.1093/emboj/17.19.5718) [Medline](#)

61. L. J. Ng, S. Wheatley, G. E. O. Muscat, J. Conway-Campbell, J. Bowles, E. Wright, D. M. Bell, P. P. L. Tam, K. S. E. Cheah, P. Koopman, SOX9 binds DNA, activates transcription, and coexpresses with type II collagen during chondrogenesis in the mouse. *Dev. Biol.* **183**, 108–121 (1997). [doi:10.1006/dbio.1996.8487](https://doi.org/10.1006/dbio.1996.8487) [Medline](#)
62. E. Wright, M. R. Hargrave, J. Christiansen, L. Cooper, J. Kun, T. Evans, U. Gangadharan, A. Greenfield, P. Koopman, The *Sry*-related gene *Sox9* is expressed during chondrogenesis in mouse embryos. *Nat. Genet.* **9**, 15–20 (1995). [doi:10.1038/ng0195-15](https://doi.org/10.1038/ng0195-15) [Medline](#)
63. J. Gadi, S.-H. Jung, M.-J. Lee, A. Jami, K. Ruthala, K.-M. Kim, N.-H. Cho, H.-S. Jung, C.-H. Kim, S.-K. Lim, The transcription factor protein Sox11 enhances early osteoblast differentiation by facilitating proliferation and the survival of mesenchymal and osteoblast progenitors. *J. Biol. Chem.* **288**, 25400–25413 (2013). [doi:10.1074/jbc.M112.413377](https://doi.org/10.1074/jbc.M112.413377) [Medline](#)
64. J. Brun, O. Fromigué, F.-X. Dieudonné, C. Marty, J. Chen, J. Dahan, Y. Wei, P. J. Marie, The LIM-only protein FHL2 controls mesenchymal cell osteogenic differentiation and bone formation through Wnt5a and Wnt10b. *Bone* **53**, 6–12 (2013). [doi:10.1016/j.bone.2012.11.020](https://doi.org/10.1016/j.bone.2012.11.020) [Medline](#)
65. Z. Hamidouche, E. Haÿ, P. Vaudin, P. Charbord, R. Schüle, P. J. Marie, O. Fromigué, FHL2 mediates dexamethasone-induced mesenchymal cell differentiation into osteoblasts by activating Wnt/ β -catenin signaling-dependent Runx2 expression. *FASEB J.* **22**, 3813–3822 (2008). [doi:10.1096/fj.08-106302](https://doi.org/10.1096/fj.08-106302) [Medline](#)
66. T. Günther, C. Poli, J. M. Müller, P. Catala-Lehnen, T. Schinke, N. Yin, S. Vomstein, M. Amling, R. Schüle, Fhl2 deficiency results in osteopenia due to decreased activity of osteoblasts. *EMBO J.* **24**, 3049–3056 (2005). [doi:10.1038/sj.emboj.7600773](https://doi.org/10.1038/sj.emboj.7600773) [Medline](#)
67. T. Saito, S. Ohba, F. Yano, I. Seto, Y. Yonehara, T. Takato, T. Ogasawara, Runx1 and Runx3 are downstream effectors of Nanog in promoting osteogenic differentiation of the mouse mesenchymal cell line C3H10T1/2. *Cell. Reprogram.* **17**, 227–234 (2015). [doi:10.1089/cell.2014.0059](https://doi.org/10.1089/cell.2014.0059) [Medline](#)
68. Y. Wang, R. M. Belflower, Y.-F. Dong, E. M. Schwarz, R. J. O’Keefe, H. Drissi, Runx1/AML1/Cbfa2 mediates onset of mesenchymal cell differentiation toward chondrogenesis. *J. Bone Miner. Res.* **20**, 1624–1636 (2005). [doi:10.1359/JBMR.050516](https://doi.org/10.1359/JBMR.050516) [Medline](#)
69. M. Kundu, A. Javed, J.-P. Jeon, A. Horner, L. Shum, M. Eckhaus, M. Muenke, J. B. Lian, Y. Yang, G. H. Nuckolls, G. S. Stein, P. P. Liu, Cbfb interacts with Runx2 and has a critical role in bone development. *Nat. Genet.* **32**, 639–644 (2002). [doi:10.1038/ng1050](https://doi.org/10.1038/ng1050) [Medline](#)
70. C. A. Yoshida, T. Furuichi, T. Fujita, R. Fukuyama, N. Kanatani, S. Kobayashi, M. Satake, K. Takada, T. Komori, Core-binding factor β interacts with Runx2 and is required for skeletal development. *Nat. Genet.* **32**, 633–638 (2002). [doi:10.1038/ng1015](https://doi.org/10.1038/ng1015) [Medline](#)
71. K. S. Lee, H.-J. Kim, Q.-L. Li, X.-Z. Chi, C. Ueta, T. Komori, J. M. Wozney, E.-G. Kim, J.-Y. Choi, H.-M. Ryoo, S.-C. Bae, Runx2 is a common target of transforming growth factor beta1 and bone morphogenetic protein 2, and cooperation between Runx2 and Smad5 induces osteoblast-specific gene expression in the pluripotent mesenchymal

- precursor cell line C2C12. *Mol. Cell. Biol.* **20**, 8783–8792 (2000).
[doi:10.1128/MCB.20.23.8783-8792.2000](https://doi.org/10.1128/MCB.20.23.8783-8792.2000) [Medline](#)
72. J. Y. Beak, H. S. Kang, Y. S. Kim, A. M. Jetten, Krüppel-like zinc finger protein Glis3 promotes osteoblast differentiation by regulating FGF18 expression. *J. Bone Miner. Res.* **22**, 1234–1244 (2007). [doi:10.1359/jbmr.070503](https://doi.org/10.1359/jbmr.070503) [Medline](#)
73. Y. G. Wang, X. D. Li, Z. Y. Liu, T. G. Zhang, B. Chen, G. Q. Hou, Q. Hong, P. Xie, S. X. Du, All-trans-retinoid acid (ATRA) may have inhibited chondrogenesis of primary hind limb bud mesenchymal cells by downregulating Pitx1 expression. *Toxicol. Lett.* **224**, 282–289 (2014). [doi:10.1016/j.toxlet.2013.06.220](https://doi.org/10.1016/j.toxlet.2013.06.220) [Medline](#)
74. W. Jin, T. Takagi, S. N. Kaneshashi, T. Kurahashi, T. Nomura, J. Harada, S. Ishii, Schnurri-2 controls BMP-dependent adipogenesis via interaction with Smad proteins. *Dev. Cell* **10**, 461–471 (2006). [doi:10.1016/j.devcel.2006.02.016](https://doi.org/10.1016/j.devcel.2006.02.016) [Medline](#)
75. K. Hata, R. Nishimura, F. Ikeda, K. Yamashita, T. Matsubara, T. Nokubi, T. Yoneda, Differential roles of Smad1 and p38 kinase in regulation of peroxisome proliferator-activating receptor γ during bone morphogenetic protein 2-induced adipogenesis. *Mol. Biol. Cell* **14**, 545–555 (2003). [doi:10.1091/mbc.E02-06-0356](https://doi.org/10.1091/mbc.E02-06-0356) [Medline](#)
76. V. Sottile, K. Seuwen, Bone morphogenetic protein-2 stimulates adipogenic differentiation of mesenchymal precursor cells in synergy with BRL 49653 (rosiglitazone). *FEBS Lett.* **475**, 201–204 (2000). [doi:10.1016/S0014-5793\(00\)01655-0](https://doi.org/10.1016/S0014-5793(00)01655-0) [Medline](#)
77. J. P. Kirton, N. J. Crofts, S. J. George, K. Brennan, A. E. Canfield, Wnt/ β -catenin signaling stimulates chondrogenic and inhibits adipogenic differentiation of pericytes: Potential relevance to vascular disease? *Circ. Res.* **101**, 581–589 (2007).
[doi:10.1161/CIRCRESAHA.107.156372](https://doi.org/10.1161/CIRCRESAHA.107.156372) [Medline](#)
78. J. A. Kennell, O. A. MacDougald, Wnt signaling inhibits adipogenesis through β -catenin-dependent and -independent mechanisms. *J. Biol. Chem.* **280**, 24004–24010 (2005).
[doi:10.1074/jbc.M501080200](https://doi.org/10.1074/jbc.M501080200) [Medline](#)
79. S. E. Ross, N. Hemati, K. A. Longo, C. N. Bennett, P. C. Lucas, R. L. Erickson, O. A. MacDougald, Inhibition of adipogenesis by Wnt signaling. *Science* **289**, 950–953 (2000).
[doi:10.1126/science.289.5481.950](https://doi.org/10.1126/science.289.5481.950) [Medline](#)
80. J. R. Park, J. W. Jung, Y. S. Lee, K. S. Kang, The roles of Wnt antagonists Dkk1 and sFRP4 during adipogenesis of human adipose tissue-derived mesenchymal stem cells. *Cell Prolif.* **41**, 859–874 (2008). [doi:10.1111/j.1365-2184.2008.00565.x](https://doi.org/10.1111/j.1365-2184.2008.00565.x) [Medline](#)
81. W. Wang, X. Li, M. Lee, S. Jun, K. E. Aziz, L. Feng, M. K. Tran, N. Li, P. D. McCrea, J.-I. Park, J. Chen, FOXKs promote Wnt/ β -catenin signaling by translocating DVL into the nucleus. *Dev. Cell* **32**, 707–718 (2015). [doi:10.1016/j.devcel.2015.01.031](https://doi.org/10.1016/j.devcel.2015.01.031) [Medline](#)
82. G. Özhan, E. Sezgin, D. Wehner, A. S. Pfister, S. J. Köhl, B. Kagermeier-Schenk, M. Köhl, P. Schwillle, G. Weidinger, Lypd6 enhances Wnt/ β -catenin signaling by promoting Lrp6 phosphorylation in raft plasma membrane domains. *Dev. Cell* **26**, 331–345 (2013).
[doi:10.1016/j.devcel.2013.07.020](https://doi.org/10.1016/j.devcel.2013.07.020) [Medline](#)
83. F. H. van Tienen, H. Laeremans, C. J. van der Kallen, H. J. Smeets, Wnt5b stimulates adipogenesis by activating PPAR γ , and inhibiting the β -catenin dependent Wnt signaling

- pathway together with Wnt5a. *Biochem. Biophys. Res. Commun.* **387**, 207–211 (2009). [doi:10.1016/j.bbrc.2009.07.004](https://doi.org/10.1016/j.bbrc.2009.07.004) [Medline](#)
84. M. Nishizuka, A. Koyanagi, S. Osada, M. Imagawa, Wnt4 and Wnt5a promote adipocyte differentiation. *FEBS Lett.* **582**, 3201–3205 (2008). [doi:10.1016/j.febslet.2008.08.011](https://doi.org/10.1016/j.febslet.2008.08.011) [Medline](#)
85. A. Kanazawa, S. Tsukada, M. Kamiyama, T. Yanagimoto, M. Nakajima, S. Maeda, Wnt5b partially inhibits canonical Wnt/beta-catenin signaling pathway and promotes adipogenesis in 3T3-L1 preadipocytes. *Biochem. Biophys. Res. Commun.* **330**, 505–510 (2005). [doi:10.1016/j.bbrc.2005.03.007](https://doi.org/10.1016/j.bbrc.2005.03.007) [Medline](#)
86. M. Konishi, T. Asaki, N. Koike, H. Miwa, A. Miyake, N. Itoh, Role of Fgf10 in cell proliferation in white adipose tissue. *Mol. Cell. Endocrinol.* **249**, 71–77 (2006). [doi:10.1016/j.mce.2006.01.010](https://doi.org/10.1016/j.mce.2006.01.010) [Medline](#)
87. T. Asaki, M. Konishi, A. Miyake, S. Kato, M. Tomizawa, N. Itoh, Roles of fibroblast growth factor 10 (Fgf10) in adipogenesis in vivo. *Mol. Cell. Endocrinol.* **218**, 119–128 (2004). [doi:10.1016/j.mce.2003.12.017](https://doi.org/10.1016/j.mce.2003.12.017) [Medline](#)
88. M. Yamasaki, H. Emoto, M. Konishi, T. Mikami, H. Ohuchi, K. Nakao, N. Itoh, FGF-10 is a growth factor for preadipocytes in white adipose tissue. *Biochem. Biophys. Res. Commun.* **258**, 109–112 (1999). [doi:10.1006/bbrc.1999.0594](https://doi.org/10.1006/bbrc.1999.0594) [Medline](#)
89. B. K. Jones, J. Levors, S. M. Tilghman, Deletion of a nuclease-sensitive region between the *Igf2* and *H19* genes leads to *Igf2* misregulation and increased adiposity. *Hum. Mol. Genet.* **10**, 807–814 (2001). [doi:10.1093/hmg/10.8.807](https://doi.org/10.1093/hmg/10.8.807) [Medline](#)
90. M. S. Sandhu, J. M. Gibson, A. H. Heald, D. B. Dunger, N. J. Wareham, Low circulating IGF-II concentrations predict weight gain and obesity in humans. *Diabetes* **52**, 1403–1408 (2003). [doi:10.2337/diabetes.52.6.1403](https://doi.org/10.2337/diabetes.52.6.1403) [Medline](#)
91. M. Borensztein, S. Viengchareun, D. Montarras, L. Journot, N. Binart, M. Lombès, L. Dandolo, Double *Myod* and *Igf2* inactivation promotes brown adipose tissue development by increasing *Prdm16* expression. *FASEB J.* **26**, 4584–4591 (2012). [doi:10.1096/fj.12-208496](https://doi.org/10.1096/fj.12-208496) [Medline](#)
92. S. B. Mortensen, C. H. Jensen, M. Schneider, M. Thomassen, T. A. Kruse, J. Laborda, S. P. Sheikh, D. C. Andersen, Membrane-tethered delta-like 1 homolog (DLK1) restricts adipose tissue size by inhibiting preadipocyte proliferation. *Diabetes* **61**, 2814–2822 (2012). [doi:10.2337/db12-0176](https://doi.org/10.2337/db12-0176) [Medline](#)
93. M. C. Mitterberger, S. Lechner, M. Mattesich, A. Kaiser, D. Probst, N. Wenger, G. Pierer, W. Zwerschke, DLK1(PREF1) is a negative regulator of adipogenesis in CD105⁺/CD90⁺/CD34⁺/CD31⁻/FABP4⁻ adipose-derived stromal cells from subcutaneous abdominal fat pads of adult women. *Stem Cell Res.* **9**, 35–48 (2012). [doi:10.1016/j.scr.2012.04.001](https://doi.org/10.1016/j.scr.2012.04.001) [Medline](#)
94. M. L. Nueda, V. Baladrón, B. Sánchez-Solana, M. A. Ballesteros, J. Laborda, The EGF-like protein dlk1 inhibits notch signaling and potentiates adipogenesis of mesenchymal cells. *J. Mol. Biol.* **367**, 1281–1293 (2007). [doi:10.1016/j.jmb.2006.10.043](https://doi.org/10.1016/j.jmb.2006.10.043) [Medline](#)

95. K. Lee, J. A. Villena, Y. S. Moon, K.-H. Kim, S. Lee, C. Kang, H. S. Sul, Inhibition of adipogenesis and development of glucose intolerance by soluble preadipocyte factor-1 (Pref-1). *J. Clin. Invest.* **111**, 453–461 (2003). [doi:10.1172/JCI15924](https://doi.org/10.1172/JCI15924) [Medline](#)
96. Y. S. Moon, C. M. Smas, K. Lee, J. A. Villena, K.-H. Kim, E. J. Yun, H. S. Sul, Mice lacking paternally expressed Pref-1/Dlk1 display growth retardation and accelerated adiposity. *Mol. Cell. Biol.* **22**, 5585–5592 (2002). [doi:10.1128/MCB.22.15.5585-5592.2002](https://doi.org/10.1128/MCB.22.15.5585-5592.2002) [Medline](#)
97. C. M. Smas, L. Chen, H. S. Sul, Cleavage of membrane-associated pref-1 generates a soluble inhibitor of adipocyte differentiation. *Mol. Cell. Biol.* **17**, 977–988 (1997). [doi:10.1128/MCB.17.2.977](https://doi.org/10.1128/MCB.17.2.977) [Medline](#)
98. C. M. Smas, H. S. Sul, Pref-1, a protein containing EGF-like repeats, inhibits adipocyte differentiation. *Cell* **73**, 725–734 (1993). [doi:10.1016/0092-8674\(93\)90252-L](https://doi.org/10.1016/0092-8674(93)90252-L) [Medline](#)
99. M. Karbiener, C. Glantschnig, D. F. Pisani, J. Laurencikiene, I. Dahlman, S. Herzig, E.-Z. Amri, M. Scheideler, Mesoderm-specific transcript (MEST) is a negative regulator of human adipocyte differentiation. *Int. J. Obes.* **39**, 1733–1741 (2015). [doi:10.1038/ijo.2015.121](https://doi.org/10.1038/ijo.2015.121) [Medline](#)
100. R. L. Mynatt, J. M. Stephens, Regulation of PPAR γ and obesity by agouti/melanocortin signaling in adipocytes. *Ann. N. Y. Acad. Sci.* **994**, 141–146 (2003). [doi:10.1111/j.1749-6632.2003.tb03173.x](https://doi.org/10.1111/j.1749-6632.2003.tb03173.x) [Medline](#)
101. R. L. Mynatt, J. M. Stephens, Agouti regulates adipocyte transcription factors. *Am. J. Physiol. Cell Physiol.* **280**, C954–C961 (2001). [Medline](#)
102. J. R. Grünberg, A. Hammarstedt, S. Hedjazifar, U. Smith, The novel secreted adipokine WNT1-inducible signaling pathway protein 2 (WISP2) is a mesenchymal cell activator of canonical WNT. *J. Biol. Chem.* **289**, 6899–6907 (2014). [doi:10.1074/jbc.M113.511964](https://doi.org/10.1074/jbc.M113.511964) [Medline](#)
103. B. Gustafson, A. Hammarstedt, S. Hedjazifar, U. Smith, Restricted adipogenesis in hypertrophic obesity: The role of WISP2, WNT, and BMP4. *Diabetes* **62**, 2997–3004 (2013). [doi:10.2337/db13-0473](https://doi.org/10.2337/db13-0473) [Medline](#)
104. T. K. Chatterjee, J. E. Basford, K. H. Yiew, D. W. Stepp, D. Y. Hui, N. L. Weintraub, Role of histone deacetylase 9 in regulating adipogenic differentiation and high fat diet-induced metabolic disease. *Adipocyte* **3**, 333–338 (2014). [doi:10.4161/adip.28814](https://doi.org/10.4161/adip.28814) [Medline](#)
105. T. K. Chatterjee, J. E. Basford, E. Knoll, W. S. Tong, V. Blanco, A. L. Blomkalns, S. Rudich, A. B. Lentsch, D. Y. Hui, N. L. Weintraub, HDAC9 knockout mice are protected from adipose tissue dysfunction and systemic metabolic disease during high-fat feeding. *Diabetes* **63**, 176–187 (2014). [doi:10.2337/db13-1148](https://doi.org/10.2337/db13-1148) [Medline](#)
106. T. K. Chatterjee, G. Idelman, V. Blanco, A. L. Blomkalns, M. G. Piegore Jr., D. S. Weintraub, S. Kumar, S. Rajsheker, D. Manka, S. M. Rudich, Y. Tang, D. Y. Hui, R. Bassel-Duby, E. N. Olson, J. B. Lingrel, S.-M. Ho, N. L. Weintraub, Histone deacetylase 9 is a negative regulator of adipogenic differentiation. *J. Biol. Chem.* **286**, 27836–27847 (2011). [doi:10.1074/jbc.M111.262964](https://doi.org/10.1074/jbc.M111.262964) [Medline](#)

107. Y. H. Chen, F.-L. Yeh, S.-P. Yeh, H.-T. Ma, S.-C. Hung, M.-C. Hung, L.-Y. Li, Myocyte enhancer factor-2 interacting transcriptional repressor (MITR) is a switch that promotes osteogenesis and inhibits adipogenesis of mesenchymal stem cells by inactivating peroxisome proliferator-activated receptor gamma-2. *J. Biol. Chem.* **286**, 10671–10680 (2011). [doi:10.1074/jbc.M110.199612](https://doi.org/10.1074/jbc.M110.199612) [Medline](#)
108. Z. C. Zhang, Y. Liu, S.-F. Li, L. Guo, Y. Zhao, S.-W. Qian, B. Wen, Q.-Q. Tang, X. Li, Suv39h1 mediates AP-2 α -dependent inhibition of C/EBP α expression during adipogenesis. *Mol. Cell. Biol.* **34**, 2330–2338 (2014). [doi:10.1128/MCB.00070-14](https://doi.org/10.1128/MCB.00070-14) [Medline](#)
109. T. Londoño Gentile, C. Lu, P. M. Lodato, S. Tse, S. H. Olejniczak, E. S. Witze, C. B. Thompson, K. E. Wellen, DNMT1 is regulated by ATP-citrate lyase and maintains methylation patterns during adipocyte differentiation. *Mol. Cell. Biol.* **33**, 3864–3878 (2013). [doi:10.1128/MCB.01495-12](https://doi.org/10.1128/MCB.01495-12) [Medline](#)